UNIVERSITY OF OKLAHOMA
GRADUATE COLLEGE

# POTENTIAL PREDICTABILITY AND IMPACTS OF SUBSEASONAL EXTREME PRECIPITATION EVENTS IN THE UNITED STATES

A THESIS
SUBMITTED TO THE GRADUATE FACULTY
in partial fulfillment of the requirements for the
Degree of
MASTER OF SCIENCE IN METEOROLOGY

By

MELANIE A. SCHROERS
Norman, Oklahoma
2020

POTENTIAL PREDICTABILITY AND IMPACTS OF SUBSEASONAL EXTREME PRECIPITATION EVENTS IN THE UNITED STATES

A THESIS APPROVED FOR THE
SCHOOL OF METEOROLOGY

BY THE COMMITTEE CONSISTING OF

Dr. Elinor Martin (Chair)

Dr. Jason Furtado

Dr. Renee McPherson

# Acknowledgments

I would like to thank my advisor, Dr. Elinor Martin, as well as my committee, including Dr. Jason Furtado and Dr. Renee McPherson. The guidance and knowledge they shared were vital to help develop this study. I would also like to thank the entire PRES$^2$iP team for data management advice and feedback given during our meetings. The opportunity to discuss questions, difficulties and methods of this study has been incredibly beneficial for my own learning and understanding. I am extremely thankful to Ty Dickinson, Ryan Bunker and Bryony Puxley for continuously providing a new perspective on my work so that I may fully understand it from multiple angles.

To all of my former and current colleagues of NWC 5700, thank you for providing laughs and much needed distractions during my time in the office. I would also like to my working-from-home office-mates, Joel McAuliffe, Amanda Burke, Dakota Hahn, Sean Ernst and many pets, for helping make a less-than-normal situation into a fun and productive workplace. Although completing my thesis during a global pandemic felt impossible, they continuously pushed me to celebrate my successes and push forward. Lastly, to all of my countless friends and family, thank you for supporting and encouraging me throughout my masters. Although the circumstances of 2020 have not been ideal, I am thankful for the support system that OU and the School of Meteorology has helped me build in order to success.

This thesis was supported by the National Science Foundation under their Resilience against Extreme Events (PREEVENTS) program, Grant #1663840.

# Table of Contents

# List Of Tables

# List Of Figures

# Abstract

Prediction of climate extremes at the S2S time scale has become a large topic of conversation between researchers and decision makers. Long duration precipitation events, lasting 14-days, may lead to devastating impacts in agriculture, transportation, infrastructure, water management and more. Yet, forecasting at this time scale lacks understanding, given that it is longer than typical weather forecasts (1-10 days) and shorter than seasonal forecasts (3+ months). Therefore, understanding the large scale features and predictability of S2S events is crucial. Most previous research focuses primarily on characteristics and impacts of short duration precipitation. In this study we investigated the variability and predictability of 14-day extreme precipitation events. Traditional methods to find variability, Principal Component Analysis (PCA) and Maximum Covariance Analysis (MCA), found large scale variability across all events, however these methods did not find unique patterns for our events. Therefore, composites of 500hPa geopotential height and precipitable water anomalous were used to investigate predictability. We found that the combination of these variables leads to better predictability but still resulted in many false alarm days, with low probability of detection. Thus, these synoptic patterns are not unique to S2S extreme events. Typical storm reports of these events were also surveyed to help analyze impacts. We found a large range of reports, from winter weather reports for West Coast events, to tropical storm reports in Southeast events. However, every region has a significant amount of flooding reports during our S2S events. Although there is still much to learn about S2S extreme precipitation events, this study contributes to the foundational knowledge of predictability and impacts to increase societal resilience to these high impact events.

# Chapter 1

# Introduction

Bridging the gap between daily forecasting and seasonal prediction has become an increasingly important topic in order to improve risk assessment for decision makers. The World Climate Research Programme created an initiative to improve prediction at the subseasonal to seasonal time frame (S2S), with one focus area being the prediction of climate extremes (Robertson et al., 2015). Early warning of climate extremes is crucial for risk mitigation. Fourteen day precipitation events may create many devastating impacts within the region affected. Impacts from these events may be felt in multiple sectors including infrastructure, agriculture, water management, transportation, and health (e.g. Curriero et al., 2001). Impact mitigation efforts made by decision makers for extreme precipitation events may take several weeks to implement. Yet, forecast skill at this time frame is lacking when compared to daily forecasts (1-10 days) or seasonal forecasts (3+ months) due to lack of understanding of the drivers of S2S extremes (Vitart et al., 2017; Brunet et al., 2010). This study is a part of a larger Prediction of Rainfall Extremes at Subseasonal to Seasonal Periods project, PRES$^2$iP. This project aims to enhance the physical understanding of the large-scale dynamics and forcing of S2S extreme precipitation events, improve our capability to predict these events, and increase communication between research and stakeholder communities with regard to extreme precipitation.

In order to start communication between decision makers and our team of researchers, a workshop was held with 22 decision makers, including: emergency mangers,

water resource managers, and tribal environmental managers, from across the United States. The goal of the workshop was to learn what mattered most to those who use, and rely on, predictions of extreme rainfall (Cwik et al., 2020). From this workshop we learned that decision makers start planning 2 weeks to 2 months before an event, and make final decisions when closer to the start of the event. When asked how to define an extreme precipitation event, there were widely varying definitions. Many answers led back to the difference between an extreme event and extreme precipitation. Although there might be extreme precipitation, this might not always result in an extreme event with many impacts (Cwik et al., 2020). Therefore, it is important to analyze impacts associated with extreme rainfall.

Thus, it is important to know all the impacts that may be associated with S2S precipitation events. Miller et al. (2008) found that flooding is the costliest of all natural disasters and therefore is of particular interest in the case of S2S events. Flooding also affects the most people and occurs the most often when compared to other weather related disasters (UN, 2015; Slater and Villarini, 2016). Furthermore, climate change may increase the risk due to flooding into the future (IPCC, 2012). Flooding can occur from many different sources including: flash flood, river basin flooding, coastal flooding, runoff or long-lasting heavy rainfall. For example, during the month of May 2015, central Texas into Oklahoma experienced a long-lived precipitation event. During the most extreme four days, May 23-26, there was a total of 2.8 billion dollars of damage, with 31 fatalities (NOAA-NCEI, 2019). This was caused by the widespread rain that had already occurred earlier in the month that created run-off conditions within the Blanco river basin. Another example is the 1993 Mississippi River Basin summer flood that resulted in an estimated $15 - $20 billion dollars of damage. Kunkel et al. (1994) found that this event had persistent large-area heavy rainfall with localized extreme rainfall, as well as above-normal soil moisture before the onset of the event. Although

these extreme events happen less frequently than daily extreme rainfall, they result in devastating damages that may take multiple years to fully recover from and therefore merit a more thorough understanding.

There is no decided definition of extreme precipitation within the current literature. Instead, the typical definition within research of extreme normally has three aspects: a metric, a time scale and a spatial scale. Many previous studies focus on extreme precipitation on daily time scales, leaving S2S time scales with little examination (Barlow et al., 2019). It has been found that daily precipitation has been increasing over the past century (Karl and Knight, 1998; Kunkel et al., 1999; Groisman et al., 2012). With most of this increase is due to the positive trend of the top 10% of all rainfall. This has the potential to aid in the increase of precipitation within extreme rainfall events. Therefore, reliable predictions at the S2S time scale of extreme precipitation events are needed in order to mitigate impacts into the future.

In order to have reliable predictions of S2S events across the CONUS, the drivers of these events must be investigated. Yet, there are very few studies that investigate S2S precipitation events across the entire CONUS with a consistent definition of extreme. There are many regional based analyses of short-lived precipitation events across the CONUS. Regional analysis can be useful when studying precipitation due to the large differences in precipitation totals, seasonality and characteristics across the CONUS. For example, Zhao et al. (2017) looked at short-lived precipitation over the entire CONUS and found there were six warm season precipitation clusters and five for the cool season. Most precipitation clusters are associated with Rossby wave propagation into the region of interest, along with moisture flux convergence in the lower troposphere. Schumacher and Johnson (2006) also looked at 24 hour events specifically over the Eastern United States. They found that most of their events were associated with mesoscale convective systems (MCS) in the warm season, strong synoptic forcing

in the cool season and that tropical systems are more likely to play a role within the Southeast. Whereas, the west coast of the United States is known for a wet season that occurs during the boreal winter (Dong et al., 2019). Flanagan et al. (2018) looked at pluvial years within the central United States, defined as a year with greater than 10% of the climatological annual total precipitation. They found that pluvial years are synoptically driven with differences in the North Great Plains and the South Great Plains. In the north, these years are have lower heights over the northwest of the region with an extended Pacific jet; the south region has lower heights across the southwest. In a case study of the drivers of the extreme precipitation event that led to the flooding in Texas and Oklahoma in May of 2015, Furl et al. (2018) found a large amount of precipitable water. This precipitable water was found before the onset of the event and then was continuously being resupplied from the Gulf of Mexico throughout the event to create a record amount of rainfall. Kunkel et al. (1994) studied the 1993 summer flood of the Upper Mississippi River Basin. The persistent rainfall throughout the region from June to August occurred due to below normal heights over the Rocky Mountains and above normal heights over the eastern United States. During this event they also experienced above-normal soil moisture and below normal evaporation that led to devastating flooding through the region. Understanding the drivers of all S2S events would be the first step in moving toward better understand the predictability of these events so that decision makers are more equipped into the future.

Jennrich et al. (2020) created a database of 14-day extreme precipitation events for six regions across the CONUS from 1981-2010. The synoptic characteristics of these events vary depending on the region. All regions have a distinct 500hPa height anomaly dipole, oriented differently in each region, as well as anomalous increase in 200hPa zonal winds and moisture flux into the respective region. Yet, the variability

of synoptic patterns, predictability and impacts of these events are still unknown. This objectives of this study are the following:

- Extend the S2S 14-day extreme precipitation event database from Jennrich et al. (2020) from 1981 to 2010 until 2018.
- Investigate the variability of synoptic features during our extreme events.
- Examine the predictability of our events by finding how often the synoptic patterns during our events are associated with non-events.
- Survey the impacts that may be occurring during our events.

# Chapter 2

# Data & Methods

## 2.1 Observations & Reanalysis

Precipitation values from the Parameter Elevation Regression on Independent Slopes Model, PRISM, were utilized to define 14-day S2S events throughout seven regions in the Continental United States(CONUS) from 1981 to 2018, defined in section 2.2. PRISM interpolates many point-observations onto a 4km grid (PRISM Climate Group, Oregon State University, 2004). This interpolation process uses elevation and weighted station measurements in order to find estimates in areas with no direct observations (Daly et al., 2008). PRISM precipitation was chosen after comparing event dates for multiple precipitation datasets: Livneh (0.0625° resolution, from 1915-2011), ERA5 reanalysis precipitation (30km resolution, from 1979 to present), as well as ERA5 that has been regridded, by bilinear interpolation, onto a 1° resolution grid (Livneh et al., 2013; Copernicus Climate Change Service (C3S), 2017). The comparison for Southern Plains events can be seen in Fig. 2.1. All four datasets find similar events throughout 1981 to 2010, thus PRISM was chosen due to its high resolution and consistency with Jennrich et al. (2020).

The European Centre for Medium-Range Forecast's ERA5 reanalysis was used for all large scale variables including 500hPa geopotential height and precipitable water (Copernicus Climate Change Service (C3S), 2017). ERA5 variables have a hourly

temporal resolution, at a spatial resolution of 0.25° with 137 vertical levels up to 1hPa. The hourly data was averaged into daily values for all 14-day events.

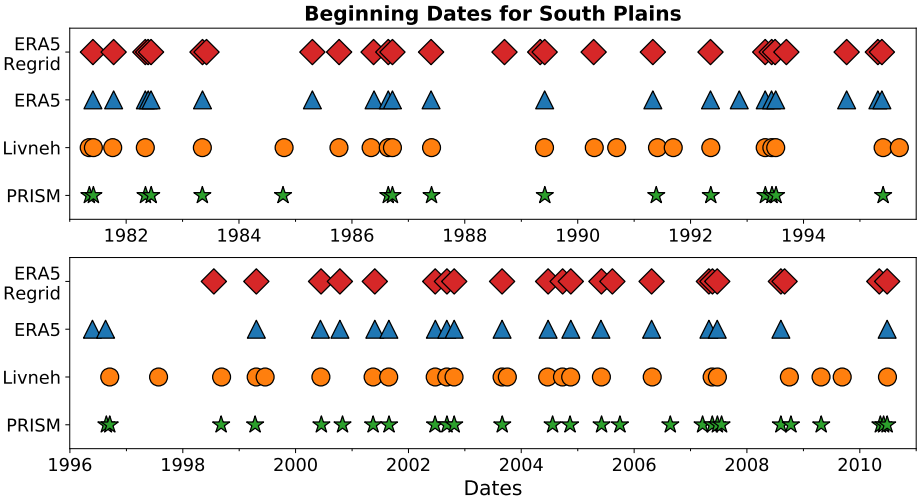


Figure 2.1: Comparison of extreme event start dates in the Southern Plains using PRISM (green star), Livneh (yellow circle), ERA5 (blue triangle) and ERA5 regridded onto a 1° resolution grid (red diamond).

## 2.2 Extreme Definition

Jennrich et al. (2020) created a database of 14-day S2S extreme precipitation events in six regions within the continental United States using PRISM precipitation from 1981-2010. The regions used in Jennrich et al. (2020) include: the Great Plains, Great Lakes, Northeast, Southeast, Mountain West and West Coast. In this study seven regions were used by splitting the Great Plains, used in Jennrich et al. (2020), into the North and South plains. This was done given that Flanagan et al. (2018) found that long term precipitation drivers differ from the North Great Plains to the South Great Plains.

The S2S extreme events were defined based on a set of criteria. First, extreme precipitation at each grid point is defined by the $95^{th}$ percentile threshold of 14-day

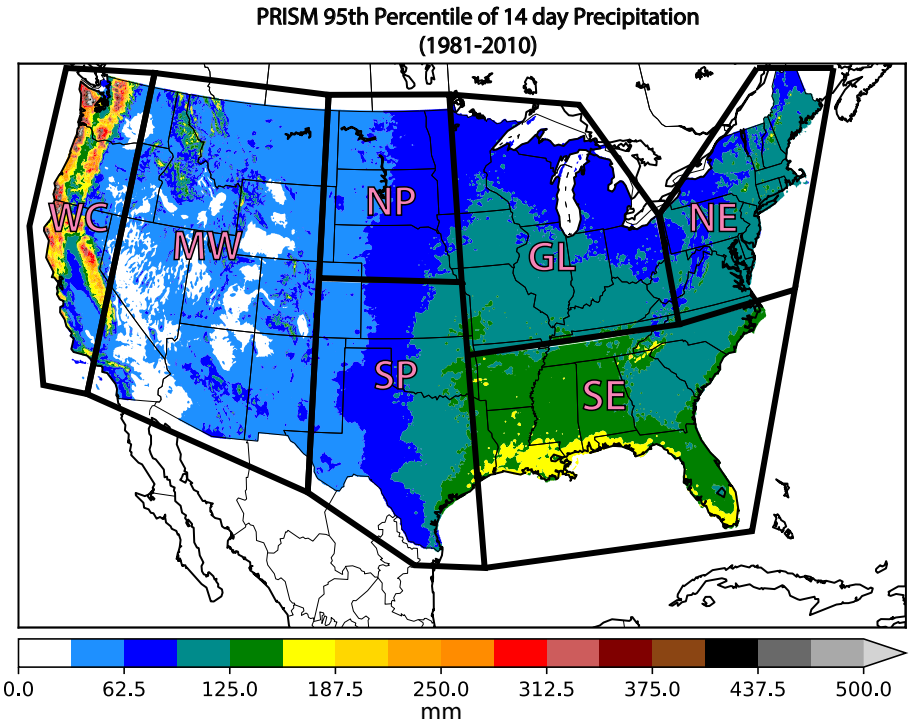


Figure 2.2: $95^{th}$ percentile of 14-day total precipitation using PRISM precipitation dataset from 1981-2010, used to determine extreme precipitation events. Shown are the seven regions in which are 14 day extreme events are found including: Northeast (NE), Great Lakes (GL), Southeast (SE), South Plains (SP), North Plains (NP), Mountain West (MW) and the West Coast (WC).

total precipitation. The seven regions of interest were divided based on similar totals for the $95^{th}$ percentile for 14-day total precipitation, seen in Fig. 2.2. Next, the total area of extreme precipitation during the 14 day sliding window must exceed a specific threshold, summarized for each region in Table 2.2. Further, if the number of days with area-averaged precipitation above 10mm per day is less than 5 days (or 3 days in MW) it is excluded. Lastly, if the heaviest precipitation day and the surrounding two days is above 50% of the events total precipitation, it is excluded. If two events are found that are overlapping, the event with the highest precipitation totals is kept. This definition was used to extend the database of S2S extreme events until 2018 with seven total regions, found in Table 2.1.

| Region | Abbreviations | Total Events | Area Threshold ($km^2$) |
|---|---|---|---|
| Northeast | NE | 38 | 200,000 |
| Southeast | SE | 46 | 300,000 |
| Great Lakes | GL | 54 | 300,000 |
| Northern Plains | NP | 17 | 200,000 |
| Southern Plains | SP | 57 | 200,000 |
| Mountain West | MW | 50 | 200,000 |
| West Coast | WC | 51 | 200,000 |

Table 2.1: Information on the seven regions used to classify our events.

## 2.3 Methods

Common synoptic patterns during all event days from 1981-2010 were found by Jennrich et al. (2020) using compositing, yet the variability within the events is still unknown. Therefore, variability is found through Principal Component Analysis (PCA) and Maximum Covariance Analysis (MCA). To define the wet and dry seasons, every region was first subjected to PCA on monthly mean precipitation. The leading mode, which explains nearly all of the variance, is representative of the region's precipitation seasonality with the principal component being positive in the wet season and negative in the dry season.

Then, PCA of extreme event day's detrended standardized geopotential height anomalies surrounding the region were used to find patterns that explain the most variance within the regions extreme events. Richman (1986) showed the use of rotated principal components led to more physically interpretable patterns. Therefore, the first three principal components, PCs, were rotated using the promax oblique method; in all regions, the leading three PCs were found to explain the majority of the field's variance (Hendrickson and White, 1964). Height anomalies over the entire CONUS were

then regressed on to the rotated standardized PCs in order to find the first two leading modes of our event days. These first two leading modes were found to be significantly different under Norths Rule for all seven regions (North et al., 01 Jul. 1982). This was then compared to composites of ERA5 500hPa geopotential height standardized anomalies for all event days within each region from 1981-2018, with a domain of 10N to 70N and 180W to 20W, similar to Jennrich et al. (2020). Significance of composites is based on a t-test at the $p < 0.05$ level.

Although heights may help to drive precipitation, moisture must also be present. Furl et al. (2018) found that the event during May 2015 within the Southern Plains had very anomalous precipitable water. Therefore, Maximum Covariance Analysis (MCA), also known as Singular Value Decomposition, was used to find coupled patterns of event day's anomalous 500hPa geopotential height and anomalous precipitable water (Bretherton et al., 1992). For each variable, we only considered the detrended variable field within the region to find the covariance matrix, $\mathrm{C} = \frac{1}{\mathrm{M}}\boldsymbol{X}^T\boldsymbol{Y}$. Where M is the total event days within the region, X is the detrended height anomaly fields and Y is the detrended precipitable water anomaly fields. The root mean squared covariance (RMSC) is larger than 0.1 for all regions. Therefore, we can say that these fields are well correlated enough to get important structures from the MCA. The leading coupled pattern of covariability was then found by regressing the height or precipitable water anomalies over the entire CONUS onto the corresponding standardized expansion coefficient time series. In order to test robustness of the coupled patterns found, the same MCA was also conducted on random non-events. Three random non-events per year, for the time period of 1981-2018, were used in the covariance matrix.

Predictability of our events using synoptic features was found by comparing the composite standardized 500hPa geopotential height anomalies during our events to all days, from 1981-2018, standardized height anomalies. As well as comparing the

composite of event days regional precipitable water standardized anomalies to all days. The domain of 10N to 70N and 180W to 20W was used for the height composites, while domain for the precipitable water composites is based on region. Comparison was done by finding congruence coefficient of each day, found in equation 2.1.

$$r_c = \frac{\sum X_{pattern} Y_{daily}}{\sqrt{\sum X_{pattern}^2 \sum Y_{daily}^2}} \tag{2.1}$$

Where $X_{pattern}$ is our composite found from our event days and $Y_{daily}$ is the daily standardize anomaly for the given day. Values of congruence coefficient are from 1 to -1, with the higher amplitude being associated with X and Y being more similar . In order to find how many events or non-events are similar to the event composites, days with congruence coefficient greater than or equal to 0.35 are counted. This threshold was chosen after sensitivity tests were conducted on its magnitude. For each region the false alarm ratio (FAR) and probability of detection (POD) were found, seen in equation 2.2 and equation 2.3 respectively. These values show how often our event day composites are seen in non-events.

$$FAR = \frac{\text{Non-event days above 0.35}}{\text{All days above 0.35}} \tag{2.2}$$

$$POD = \frac{\text{Event days above 0.35}}{\text{All event days}} \tag{2.3}$$

## 2.4 Storm Reports and Impacts

The National Centers for Environmental Information (NCEI) storm events database was utilized to understand the storm-related impacts for events that took place after 1996 (NOAA-NCEI, 2020). Previous to 1996, the only storm reports that were counted

were tornado, thunderstorm wind and hail from the storm prediction center. After 1996, 48 event types, detailed in Murphy (2018), were recorded into the storm events database. Every report is recorded based on the county of occurrence by a National Weather Service forecast office (WFO) and then passed onto NCEI. Each storm report is defined based on the region of occurrence, which can lead to multiple definitions of the same report. For example, the amount of precipitation that may result in a flood report in the MW, may not result in a flood report in the SP due to the regional differences of precipitation. Flood, Flash Flood and Heavy rainfall storm reports were of particular interest for our extreme rainfall events. These three storm reports are all indicative of loss of life or property due to excessive precipitation (Murphy, 2018). The storm data guidelines for these three reports can be seen in Table 2.4.

Storm reports are analyzed for each region to look at common storm-related impacts that occur during our extreme events. These reports are categorized by county and therefore are split into our seven regions by nearest state boundaries, seen in Fig. 2.3. The geopolitical boundaries used are similar to the boundaries used to define the seven regions. The largest discrepancy is seen in Southern California. By the event definition this area is within the MW, but by geopolitical boundaries it is within WC. This area

| Report type | Storm data guidelines |
|---|---|
| Flash Flood | "A life-threatening, rapid rise of water into a normally dry area beginning within minutes to multiple hours of causative event." |
| Flood | "Any high flow, overflow, or inundation by water which causes damage." |
| Heavy Rain | "Unusually large amount of rain which does not cause a Flash Flood or Flood event, but cases damage, e.g., roof collapse or other human/economic impact." |

Table 2.2: NWS guidelines for entering storm reports on flash flood, flood and heavy rainfall.

receives very little precipitation overall and therefore did not change the storm reports seen.

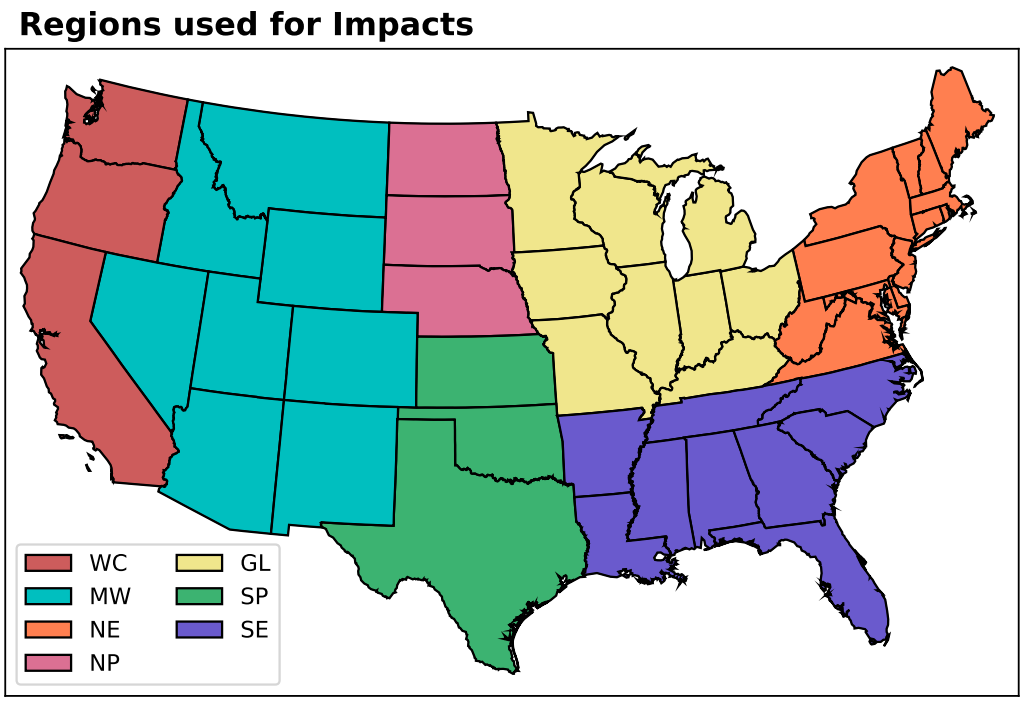


Figure 2.3: Geopolitical boundaries used to find regional NCEI storm reports for event days.

For each region, reports that have more than 100 occurrences during all events were summarized. The three storm reports related to precipitation, seen in Table 2.4, were counted by region for our event days and random days from 1996-2018 and tested for significant difference using a permutation test with 1000 iterations at a $p < 0.1$ level. Although storm reports do not give the exact impacts that may be experienced on the ground, they can assist with overall storm type. Knowing the typical storm reports of extreme precipitation events, can help decision makers know what impacts may occur during the events.

# Chapter 3

# Extreme Precipitation Events Regional Analysis

The climatology of events does not differ greatly from Jennrich et al. (2020), but here we summarize a total of 367 events found throughout seven regions from 1981-2018. The yearly distribution of events from 1981-2010 nearly match with what was found in Jennrich et al. (2020), as seen in Fig. 3.1. The only difference from 1981-2010 is an effect of splitting the Great Plains into the NP and SP. This resulted in many more events in the SP, total of 57 events, than in the NP with a total of 17 events (Table 2.1). Most of the NP events are seen at the end of the time frame, with 8 of 17 occurring after 2010. When looking at all regions combined from 2011-2018, we see 6 years that have at least 10 events or more, while in the previous 30 years there were only 7 years total with 10 or more events. The monthly distribution of events per region also matches closely with what was found in Jennrich et al. (2020). The GL, NP and SP have a bimodal distribution with maximums in June and early fall, just as seen as in the GL and the Great Plains in Jennrich et al. (2020). By contrast, the NE and SE had events throughout the entire year. Finally, the WC and MW have almost all of their events within the winter months. In the following sections we will discuss each region separately in order to highlight the similarities and difference between each region. Following the regions, tropical cyclone (TC) activity and impacts will be discussed.

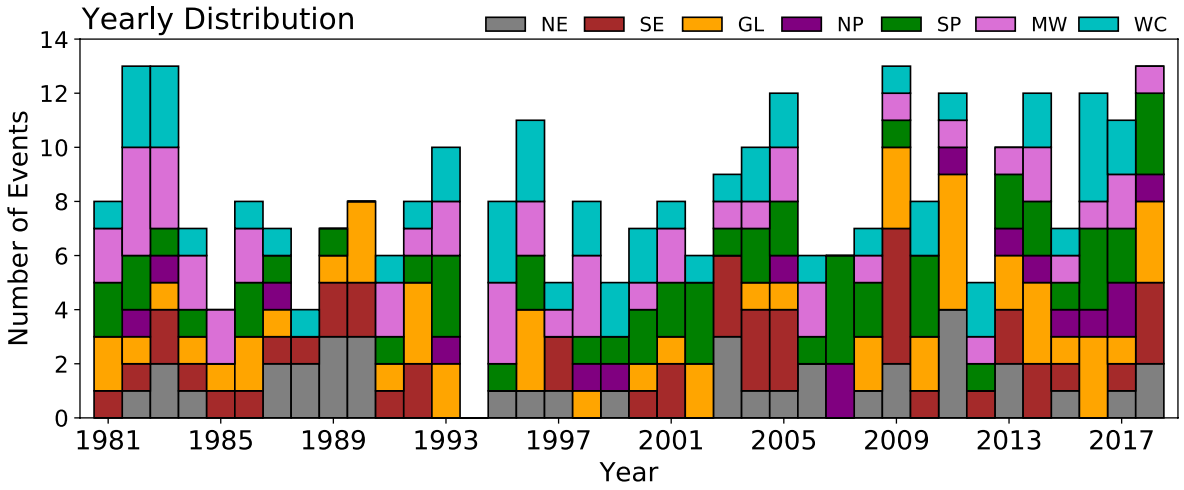


Figure 3.1: Distribution of 14-day extreme precipitation events, from 1981-2018, by year for all seven regions, color coded.

## 3.1 Northeast

The NE had a total of 38 events from 1981-2018. The events occurred about once a year, with 2011 having the most with 4 total events. During these events within 2011 we saw: two tropical systems, a persistent storm track and record snowfall for January. These events helped to produce a record-breaking wet year within the NE in 2011 (NOAA-NCEI, 2011). The leading mode of average monthly precipitation within the NE is a wet season from April to October. Nearly 30 events lie within the regions wet season (Fig. 3.2) with the maximum of seven events happening within June. However, there is a secondary maximum of over 3 total events in November within the dry season. Events that occur within the dry season may lead to differing impacts than during the wet season, given that the cool months can bring winter precipitation.

Large scale variables can play a large role in the development of precipitation and therefore are important to understand for predictability. Therefore, the composite of standardized 500hPa geopotential height anomalies of all event days from 1981-2018 is

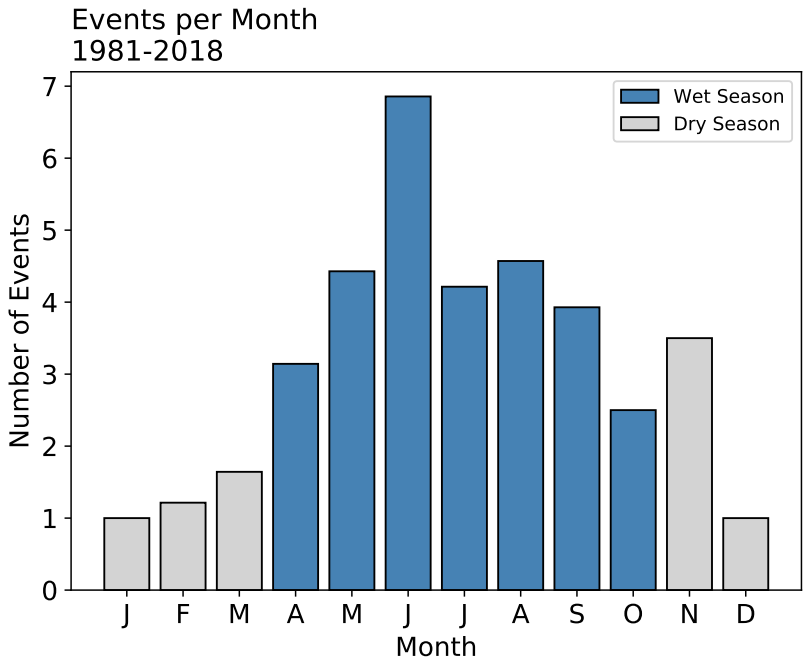


Figure 3.2: Number of extreme events days per month in the Northeast from 1981-2018. The Wet season is seen in blue, April through October, while dry seasons is seen in grey, November through March.

seen in Fig. 3.3a. This pattern matches with what was found in Jennrich et al. (2020) with a trough-ridge dipole centered over the region. The trough is seen to the west of the region, while the ridge is to the east. This synoptic pattern is favorable for precipitation in a quasi-geostrophic framework due to positive differential vorticity advection and warm air advection supporting rising motion within the region (Bluestein, 1992). Fig. 3.3b-c show the first and second leading modes of our event days standardized height anomalies. The leading mode, explaining 46.06% of the variance, is a large anomaly centered at the bottom of the region with an anomaly of opposite sign to the northeast of the region. The second leading mode contains a North/South oriented dipole of anomalies, that explains 23.38% of the variance. These patterns look more similar to large scale variability that may be occurring over the region during our events, and therefore may not be unique height patterns to our event days.

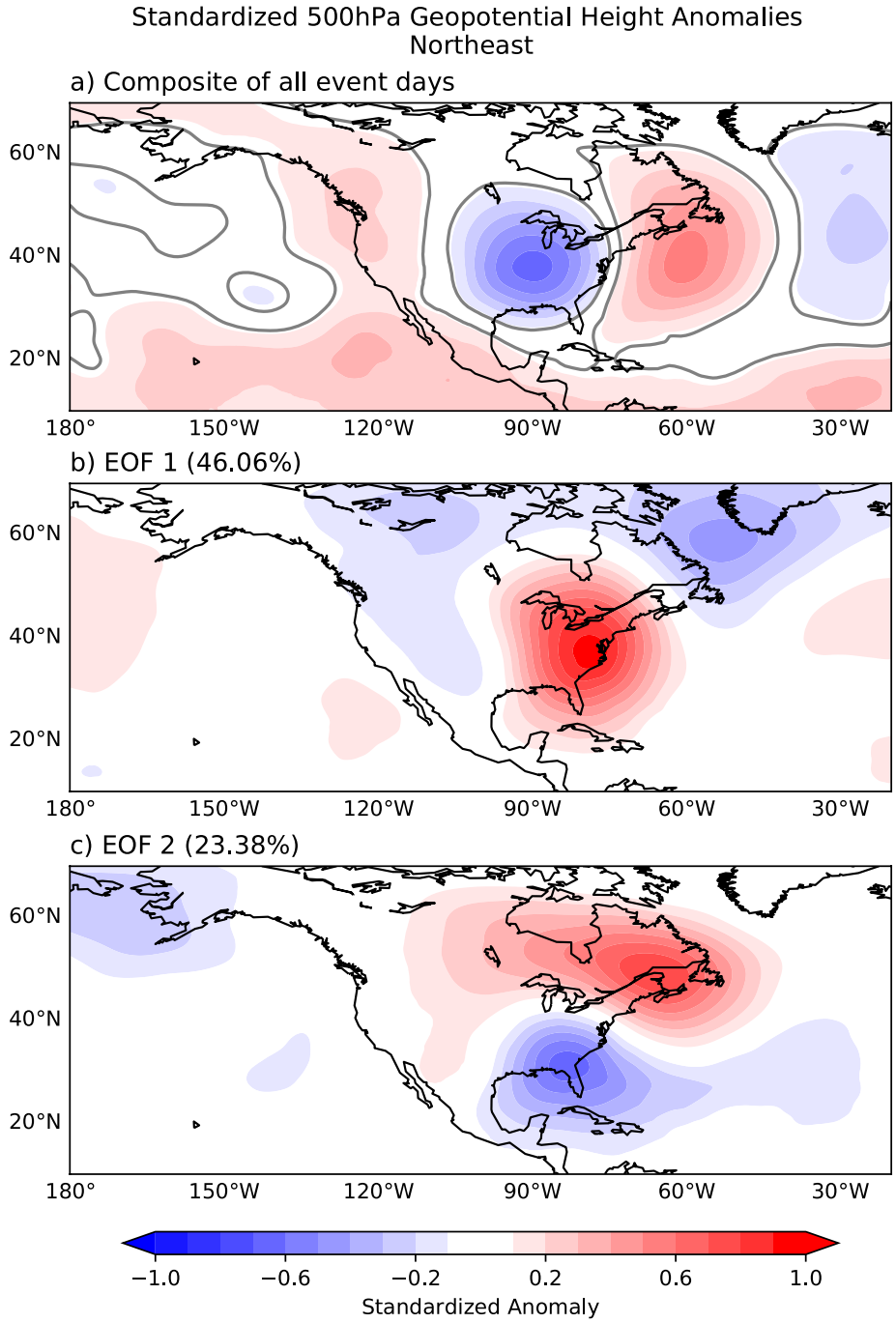


Figure 3.3: (a) Composite of all event days standardized 500hPa geopotential height anomalies (HGTa). Significance from a t-test at the $p < 0.05$ level is shown as a gray contour. (b) Regression of HGTa onto the first standardized PC time series and (c) onto the second standardized PC time series of all event days HGTa. Variance explained can be found in the titles of (b) and (c).

Potential predictability of the events, using heights, is assessed by comparing all days standardized height fields to the event day's height composite, Fig. 3.3a. An example time series of congruence coefficient for three years is shown in Fig. 3.4. The three years chosen for NE are 1988-1990, when 8 total events occurred. Although, there are maximums found during our events, as expected there are also maximums found outside of our events. This indicates that this pattern is not unique to our events. For example, the event that occurred in June of 1989 has a maximum congruence coefficient of near 0.6, yet this same magnitude is seen at the very beginning of 1988 without a precipitation event. To look at the entire time frame of 1981-2018 a contingency table was made of all event days (Table 3.1). A congruence coefficient value of 0.35 was chosen as a threshold to examine predictability of our events. We found that 20% of events days passed the threshold, whereas only 6.4% of all non-event days passed. Therefore, the probability of detection in the NE with 500hPa heights alone is 20%, while, the false alarm ratio (FAR) of NE events is 89%.

| | Event days | Non-Event days |
|---|---|---|
| Above Threshold | 106 | 858 |
| Below Threshold | 426 | 12480 |

Table 3.1: Contingency table for congruence coefficient for heights alone. Non-events are any day that is not within the extreme events in the NE. The threshold for congruence coefficient is set as 0.35

In order for precipitation to occur we must have a source of lift and moisture. Therefore, coupled patterns of our event days 500hPa geopotential height and precipitable water fields were found using MCA. The coupled patterns and corresponding expansion coefficient time series for the NE are shown in Fig. 3.5. The leading mode of covariability explains 67.6% of the total covariance. It shows a large positive height

anomaly over the region with a corresponding positive precipitable water anomaly that extends the entire east coast. High geopotential height anomalies are associated with ridging throughout the region. This can lead to warmer temperatures and more potential for moisture. Therefore, it follows that we would have a large precipitable water anomaly aligned with the height anomaly. When comparing the expansion coefficient

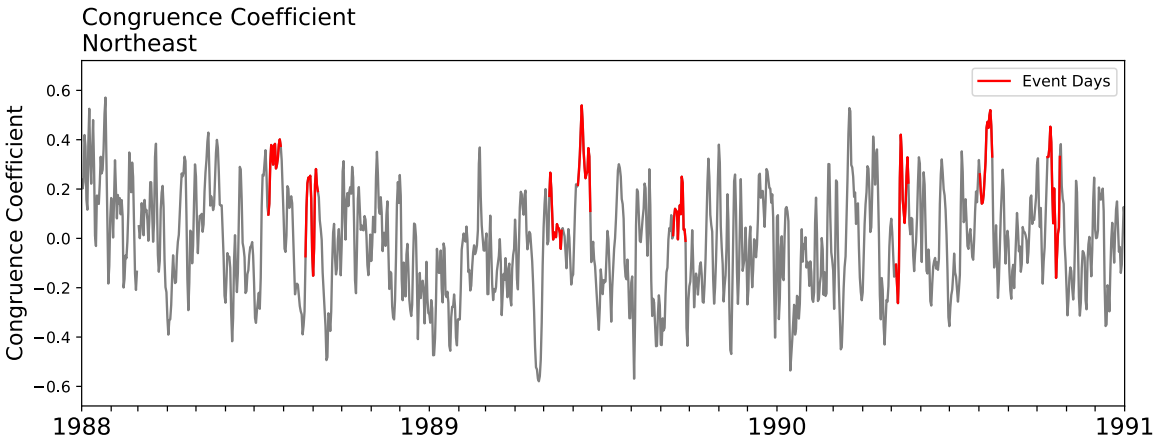


Figure 3.4: Time Series of congruence coefficient comparing the height field composite, 3.3a, to height fields of all days in three years that experienced many events within the NE. Events are seen in red, while non-events are seen in grey.

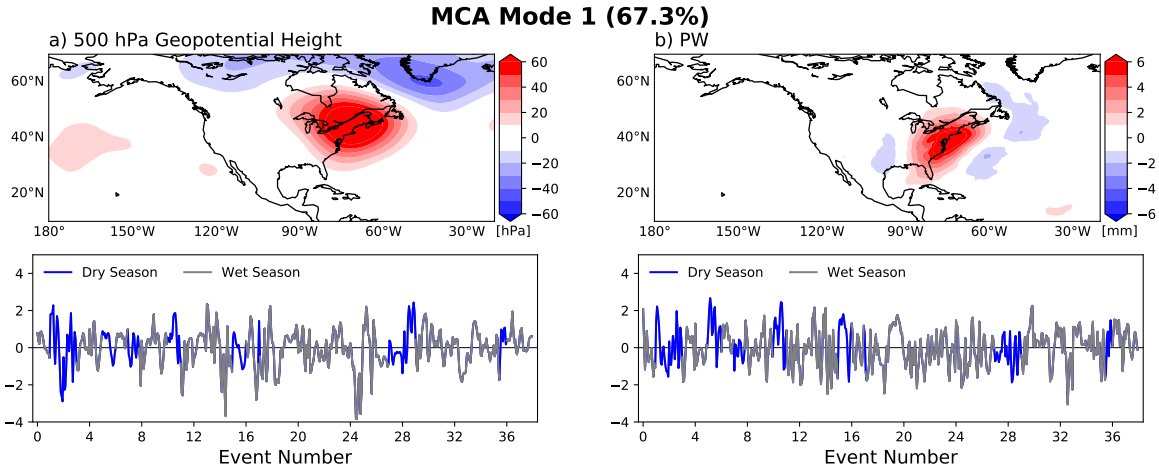


Figure 3.5: Spatial patterns of geopotential height (left, a) and precipitable water (right, b) of the first mode of the MCA of NE event days, with their respective time series of expansion coefficients under the spatial maps. Events are color coded based on if the event occurred within the NE wet or dry season.

time series of all events there is not a distinct difference between wet and dry season events. It is also interesting to note that the height pattern found from the MCA, Fig. 3.5a, is very similar to the leading mode found in the PCA, Fig. 3.3b. However, it was seen that when conducting the same MCA on random non-event days we get the same patterns, Fig. A.8. This suggests that these patterns are not unique for our extreme events and instead explaining the overall variance of the region.

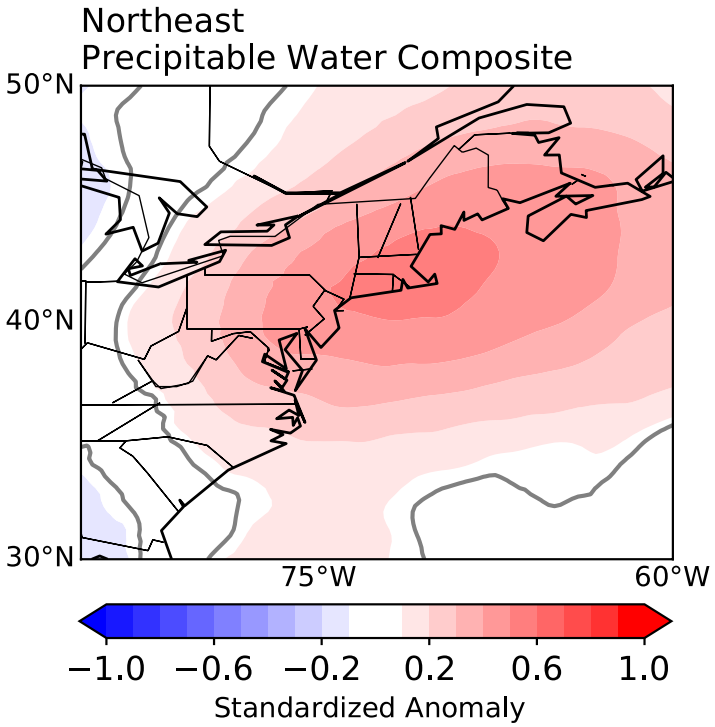


Figure 3.6: Composite of all event days standardized precipitable water anomaly. Significance from a t-test at the $p < 0.05$ level is shown as a gray contour.

Since using heights alone leads to very high FAR in our events, we instead looked at predictability when using multiple variables. Similar to heights alone, we want to find the number of days above a congruence coefficient of 0.35 when comparing all days fields to the composite of heights and to the composite of precipitable water, seen in Fig. 3.6. The precipitable water composite shows that there is a significant positive anomaly over the region during NE events. Thus, we want to see how often we have

anomalous precipitable water along with a trough-ridge pattern that results in an event or a non-event. A contingency table of all days from 1981-2018 is seen in Table 3.2. With the addition of precipitable water our POD falls to 12.6% from a previous POD of 20% with heights alone. Our FAR of NE events only decreases to 87.6% from 89%. Therefore, the addition of precipitable water did not change the predictability of NE events much.

| | Event days | Non-Event days |
|---|---|---|
| Above Threshold | 67 | 475 |
| Below Threshold | 465 | 12863 |

Table 3.2: Contingency table for congruence coefficient for 500hPa heights and precipitable water. Non-events are any day that is not within the extreme events in the NE. The threshold for congruence coefficient is set as 0.35

## 3.2 Southeast

The SE had a total of 46 events from 1981-2018. From 1981 to 1992 there was at least one event that occurred in the region. Although events no longer happened every consecutive year, there were many years from 1992-2018 that had more than one event, with a maximum in 2009 with 5 events. As seen in Fig. 3.7, there is no specific wet season in the SE. This is consistent with Schumacher and Johnson (2006) who also saw 24 hour precipitation events can occur within any season in the SE. Therefore, it follows that the events are distributed throughout the year with a peak during May and June and another during the cool months of November to February.

The composite of standardized 500hPa geopotential height anomalies of all event days within the SE show a similar pattern to the NE. There is a trough to the east of

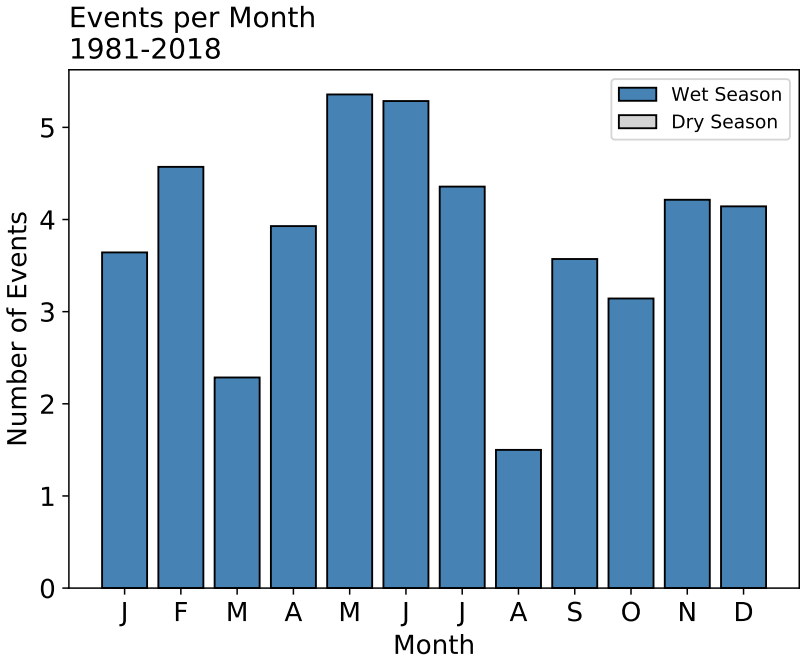

Figure 3.7: As in figure 3.2 but for the SE.

the region, with a ridge to the west, shown in Fig 3.8a. Similar to the NE, this pattern does support rising motion and could in turn produce precipitation. In contrast, the leading mode, that explains 50.7% of the variance, is a large anomaly centered on the top of the region, Fig 3.8b. There is also another anomaly, lower in magnitude, surrounding the larger anomaly to the north. The second leading mode, explaining 20.1% of the variance, looks much more similar to the composite with a trough-ridge dipole oriented east/west over the region, Fig 3.8c. These patterns match very closely to the leading modes within the NE and therefore increase the possibility that we are finding large scale variability and not variability within our extreme events.

To investigate how often the height pattern found in the composite is seen during events and non-events we looked at a time period of 2003 to 2005. During this time the SE experienced 9 events. As seen in the NE, we again see maximums during our events, as well as during non-events, Fig. 3.9. From table 3.2, we see that 19% of

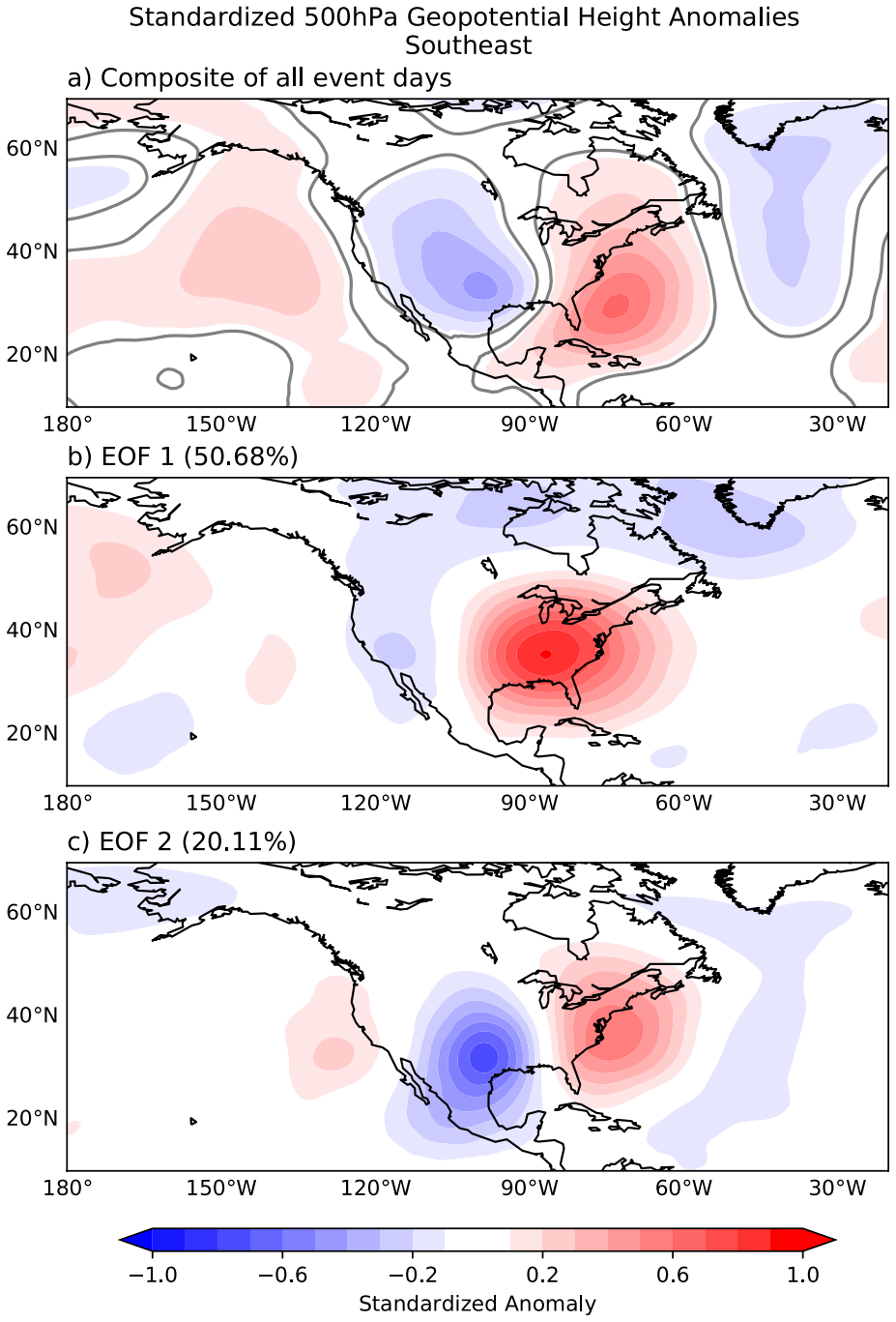


Figure 3.8: As in figure 3.3 but for the SE.

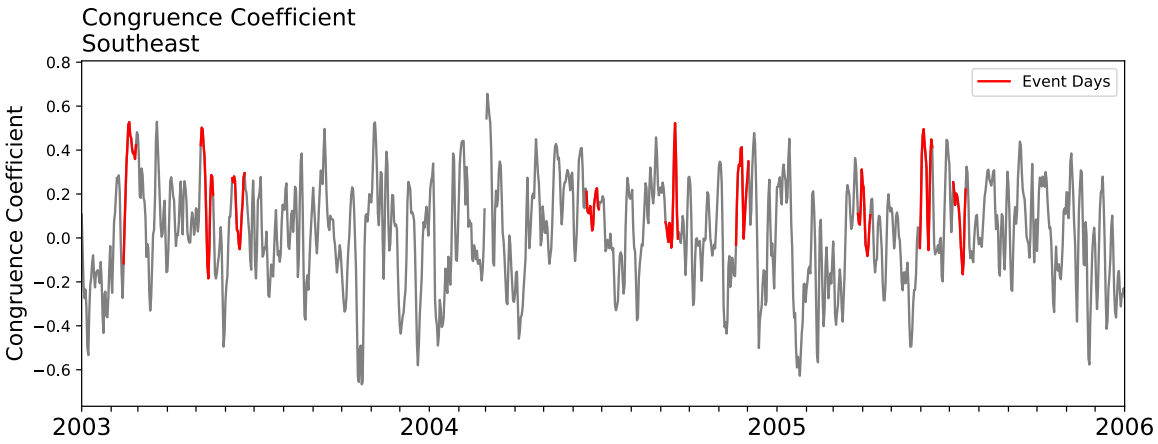


Figure 3.9: As in figure 3.4 but for the SE.

event days are above 0.35, while only 5.5% of non-event days are above the threshold. Despite events having larger congruence coefficients, there are still many days overall that have passed the threshold, 719 days, without being considered an extreme event. Therefore, the FAR of the SE is 85% while the POD is only 19%. This shows very little overall skill in predictability of our events, but we are only using one variable. Thus, it may be useful to use precipitable water as well.

| | Event days | Non-Event days |
|---|---|---|
| Above Threshold | 122 | 719 |
| Below Threshold | 522 | 12507 |

Table 3.3: As in table 3.1 but for the SE.

The coupled patterns between geopotential height and precipitable water, with their respective expansion coefficient time series, for the SE can be seen in Fig. 3.10. These patterns are very similar to the patterns found for the NE, the primary difference is the location of the maximum, which is located centered over the SE region. We still see that the precipitable water anomaly aligns well with where the ridging is occurring in the height pattern. When investigating the time series of the expansion coefficients, we

see that many event days have negative expansion coefficients for geopotential height. This indicates that there is troughing occurring during the events. This matches closely to the composite found for geopotential height. However, the MCA for random days matches closely to the pattern found for our event days, Fig. A.9. Similar to the NE, these fields are not unique to our event days.

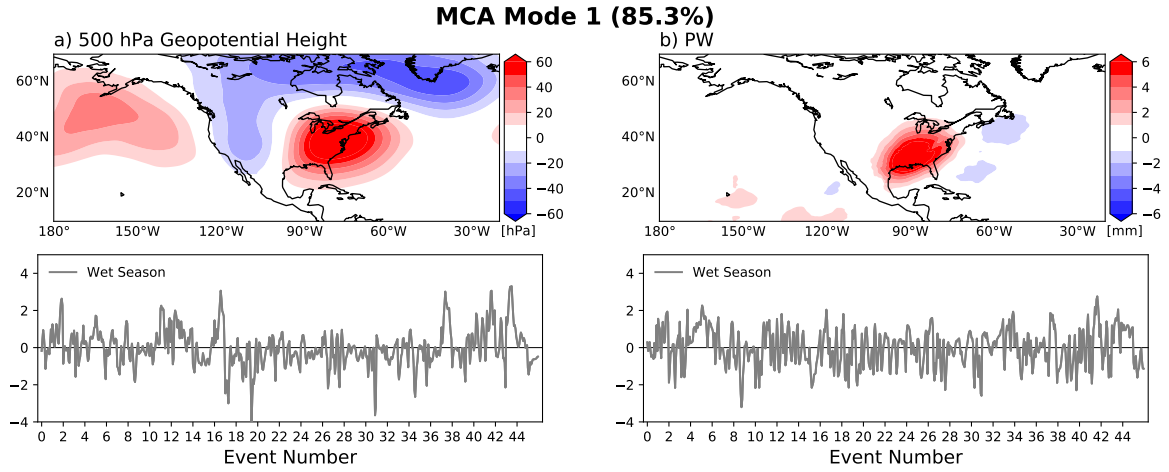


Figure 3.10: As in figure 3.5 but for the SE.

The composite of precipitable water during the SE events is seen in Fig. 3.11. As expected, we see a large positive anomaly of precipitable water over the area, similar to the leading mode found in 3.10b. Contingency table of all days from 1981-2018 made from combing congruence coefficient of all days height field and precipitable water fields is seen in Table 3.4. The POD found is 16%, while the FAR is 83%. Therefore, the FAR only decrease a small amount when using both variables, which is not a large improvement of predictability. Overall, the composite patterns found are not skillful in finding events alone, but instead are found in both event and non-event days within the SE.

| | Event days | Non-Event days |
|---|---|---|
| Above Threshold | 104 | 506 |
| Below Threshold | 540 | 12720 |

Table 3.4: As in table 3.2 but for the SE.

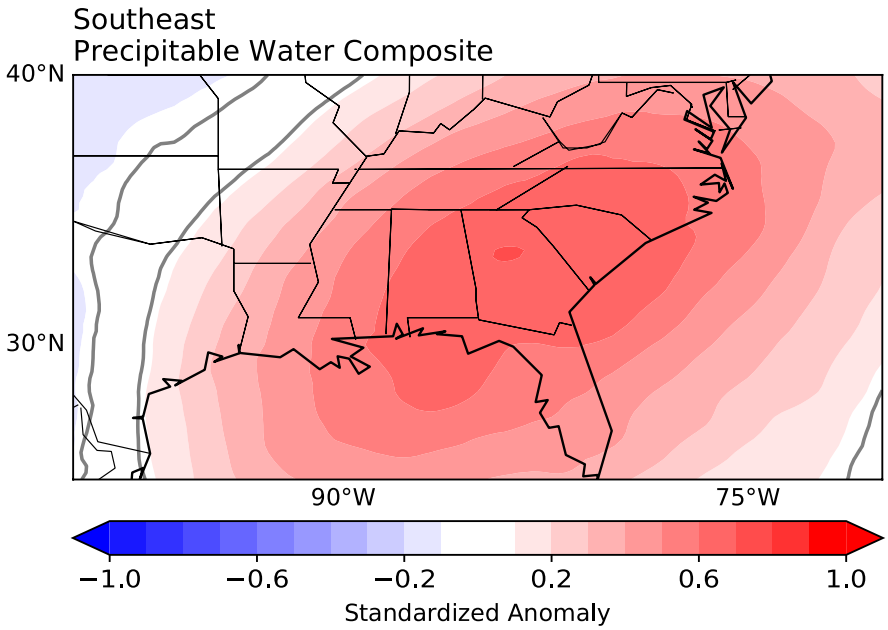


Figure 3.11: As in figure 3.6 but for the SE.

## 3.3 Great Lakes

The GL has a total of 54 events, with one or two events happening in most years. Toward the end of the time frame, years that experience more than two events become more frequent. The wet season of this region is during the warm season, from April to September. There are two maximums that happen during the wet season, one in June and another in September, seen in Fig. 3.12. There are events that happen during the dry season, with more than 4 events occurring in October. During the boreal winter (DJF) the GL experienced very few events during the time period analyzed. Therefore, there are probably not many events due to winter precipitation.

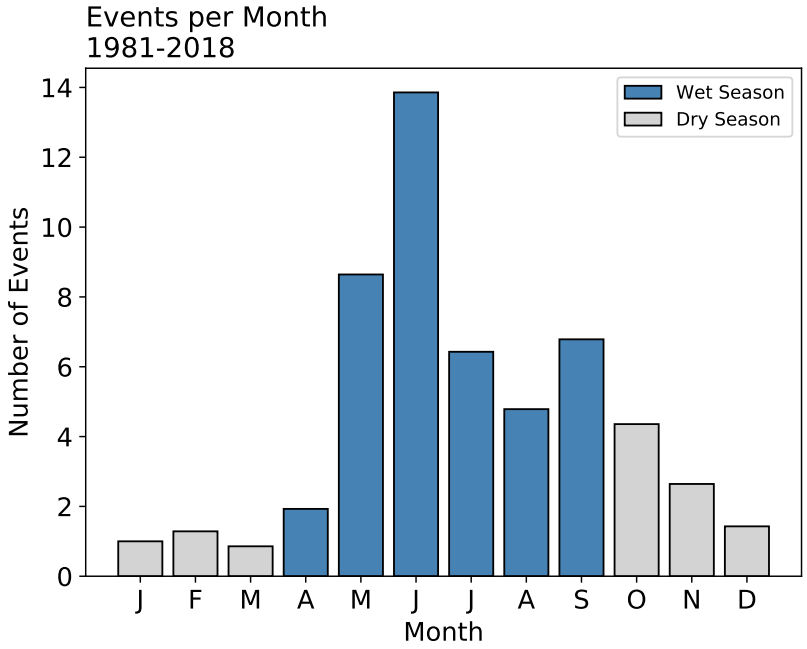


Figure 3.12: As in figure 3.2 but for the GL.

During the events in the GL the average geopotential height pattern is a trough to the northwest and a ridge to the southeast, Fig. 3.13a. There is also significant ridging in the North Pacific. Once again, this is a synoptic setup that is ideal for precipitation. Again, the leading mode of all event days within the GL is a large anomaly centered over the region, Fig. 3.13b. While the second mode is an anomaly dipole oriented north/south over the region, Fig. 3.13c.

From 2009 to 2011, the GL experienced 10 events. Therefore, an example time series of congruence coefficient for this time period is seen in Fig. 3.14. Many events, seen in red, are associated with a local maximum in congruence coefficient; but there are three events that do not have a maximum. Yet, when analyzing all days congruence coefficient we see that 30% of all event days lie above the threshold of 0.35, while only 9% of non-events is above the threshold, Table 3.5. When compared to other regions, both of these frequencies are greater. This results in a POD of 30%, while the FAR

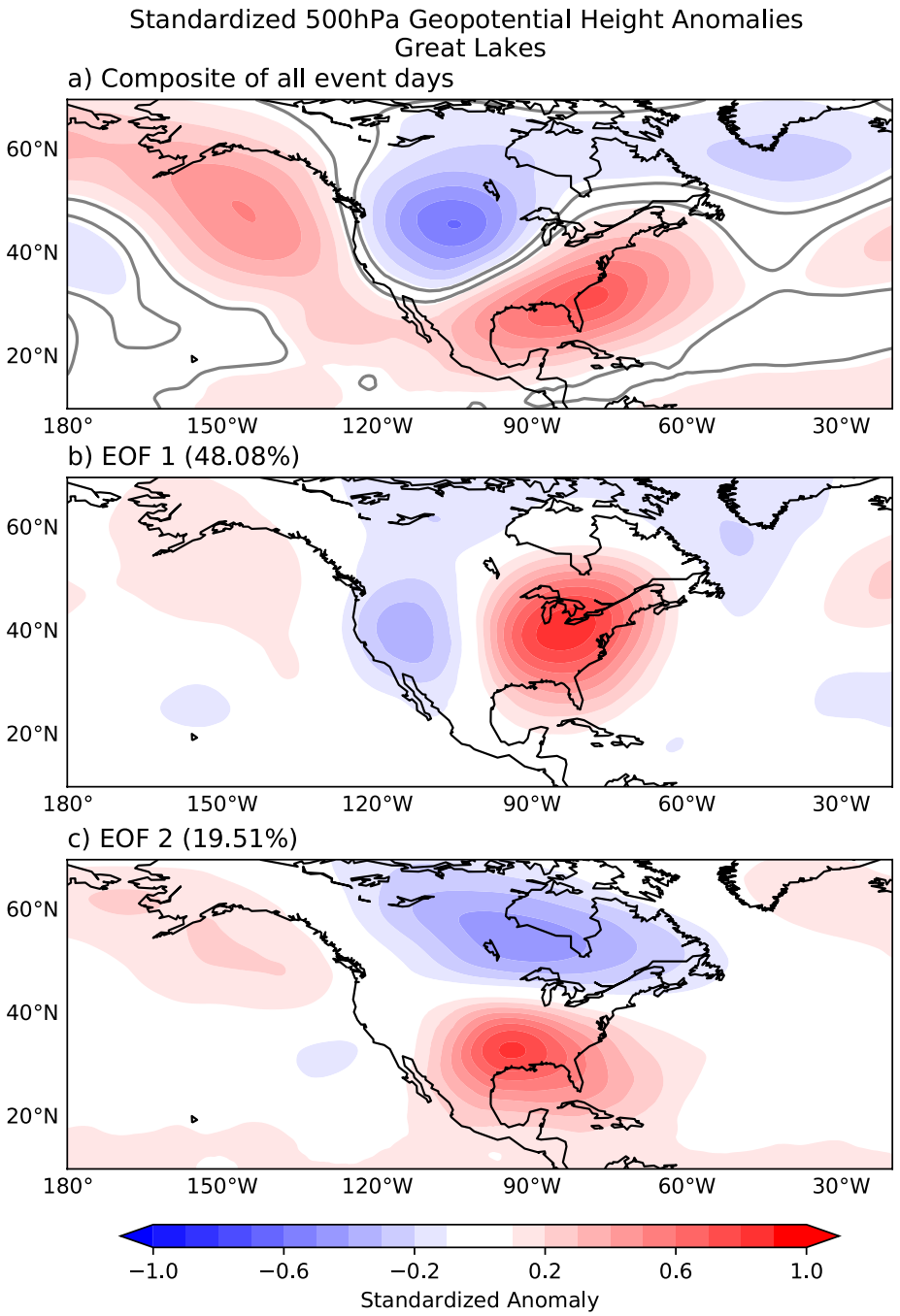


Figure 3.13: As in figure 3.3 but for the GL.

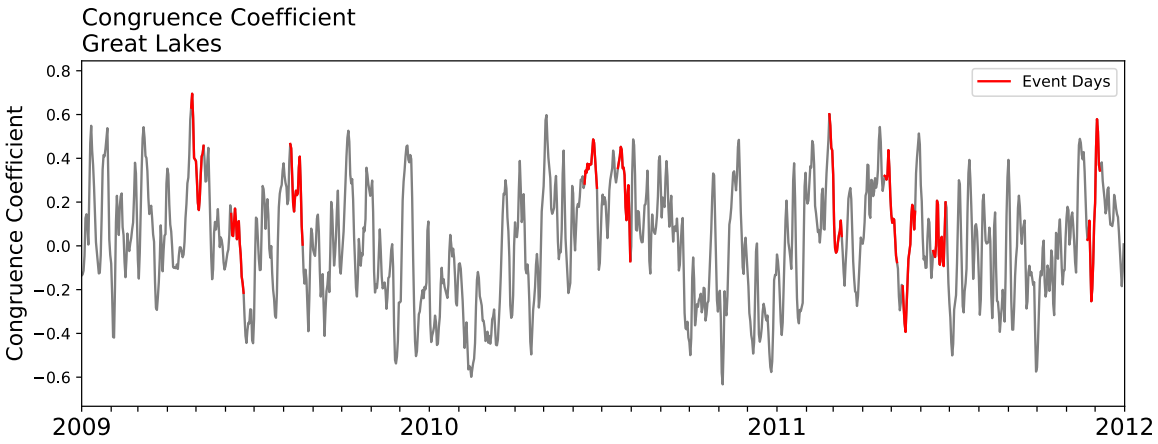


Figure 3.14: As in figure 3.4 but for the GL.

is 84%. Thus, there are many days, 1206, that have a height pattern similar to the height composite of GL events that are non-events.

| | Event days | Non-Event days |
|---|---|---|
| Above Threshold | 228 | 1206 |
| Below Threshold | 528 | 11908 |

Table 3.5: As in table 3.1 but for the GL.

The leading mode of the MCA between geopotential height and precipitable water, again, is a large anomaly within the region for both fields. The fraction of covariance explained is 81.6%, seen in Fig. 3.15. As in the NE and the SE, the GL also has a negative anomaly that is wrapped around the large positive to the north of the region. We also see that the precipitable water anomaly is aligned with the large positive height anomaly. There is also no distinct difference in expansion coefficient magnitude for the wet versus dry season in either field. As in the SE and NE, the MCA for random days matches the patterns found in our events and is therefore not unique to our events, Fig. A.10.

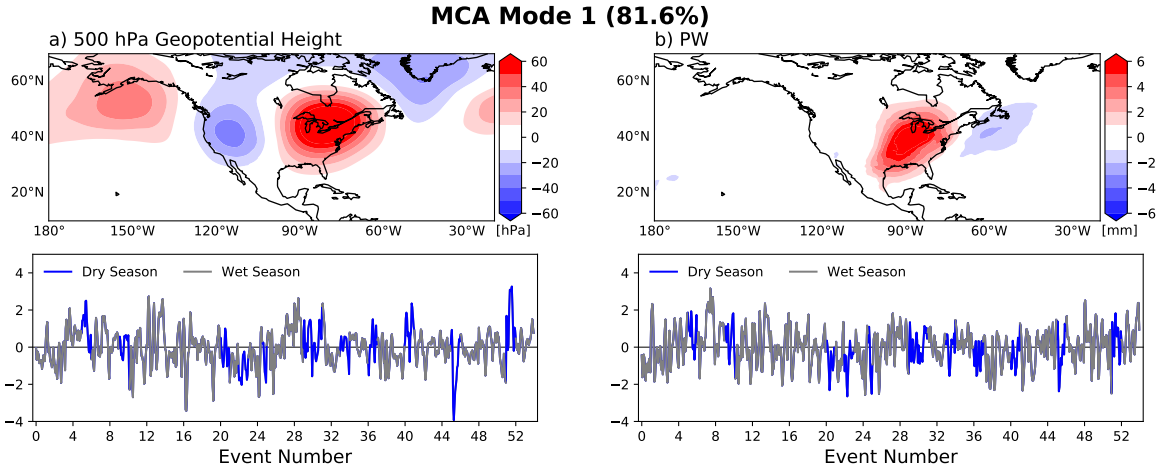


Figure 3.15: As in figure 3.5 but for the GL.

When utilizing the event day's height and precipitable water composite within the GL we see slightly more skill in predictability. The composite of GL events precipitable water field shows a anomalous precipitable water within the region, seen in Fig. 3.16. Therefore, we want to find days within 1981-2018 that have high precipitable water as well as a trough-ridge dipole of height anomalies seen in the height composite. The contingency table summarizing all days are found in Table 3.6. The POD found when using both variables is 22%, which is smaller than with heights. Yet, the total number of false alarm days decreases greatly from 1206 days to only 606 days when utilizing both variables. This decrease is also seen in the FAR of 78%. Although this is an improvement in false alarms, we are still missing 589 event days that are not seen as hits.

| | Event days | Non-Event days |
|---|---|---|
| Above Threshold | 167 | 606 |
| Below Threshold | 589 | 12508 |

Table 3.6: As in table 3.2 but for the GL.

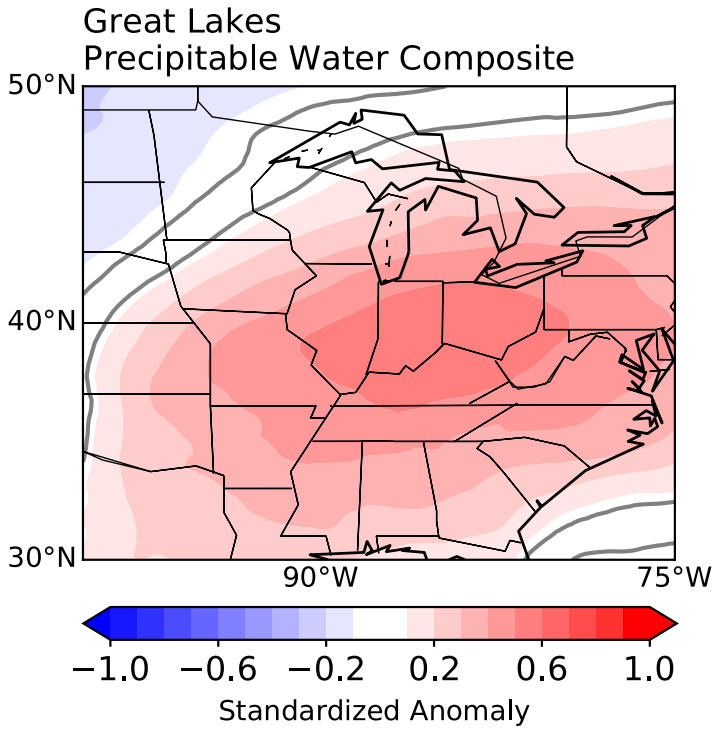


Figure 3.16: As in figure 3.6 but for the GL.

## 3.4 North Plains

The NP had the fewest total of events with only 17 throughout the entire time frame. The low event count might be resulting from the area threshold used to classify our events in this region, seen in table 2.1. The NP is the smallest region of the seven, so it might be difficult for this area threshold to be met. Almost half of these events occurred after 2010, which means NP events are infrequent from 1981-2010. We did find a distinct wet season from April to September. Almost all events fall in the wet season, with the exception of 35 event days. The maximum number of events falls in May and June.

Similar to the previous regions, the composite of all event days within the NP has a trough-ridge pattern centered over the region which is supportive of precipitation,

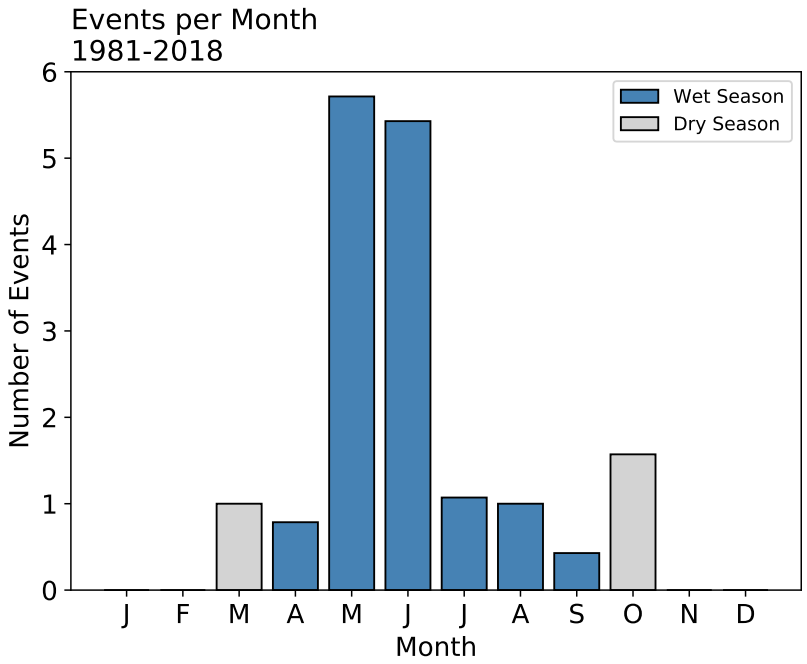

Figure 3.17: As in figure 3.2 but for the NP.

Fig. 3.18a. There is also significant ridging over Canada as well as off of the west coast. The leading mode of event days, explaining 48.52% of the total variance, is a large anomaly centered on the region, Fig. 3.18b. While the second mode, explaining 22.87% of the variance, is a anomaly dipole over the region, Fig. 3.18c. Again these patterns, are similar to all region's event days variability. Therefore, these patterns may be associated with large scale variability instead of event variability.

Predictability of the NP is going to be more difficult to access than other regions, due to the low overall event count. The time period of 2016 to 2018 was chosen to analyze a time series of congruence coefficient, Fig. 3.19. During this time period the NP experienced four events, which is the most events during a three-year time period for the NP. These four events all have positive congruence coefficient, with three events having local maximums. However, there are many days outside of the events that have maximums similar to our events. When looking at the congruence coefficient for all

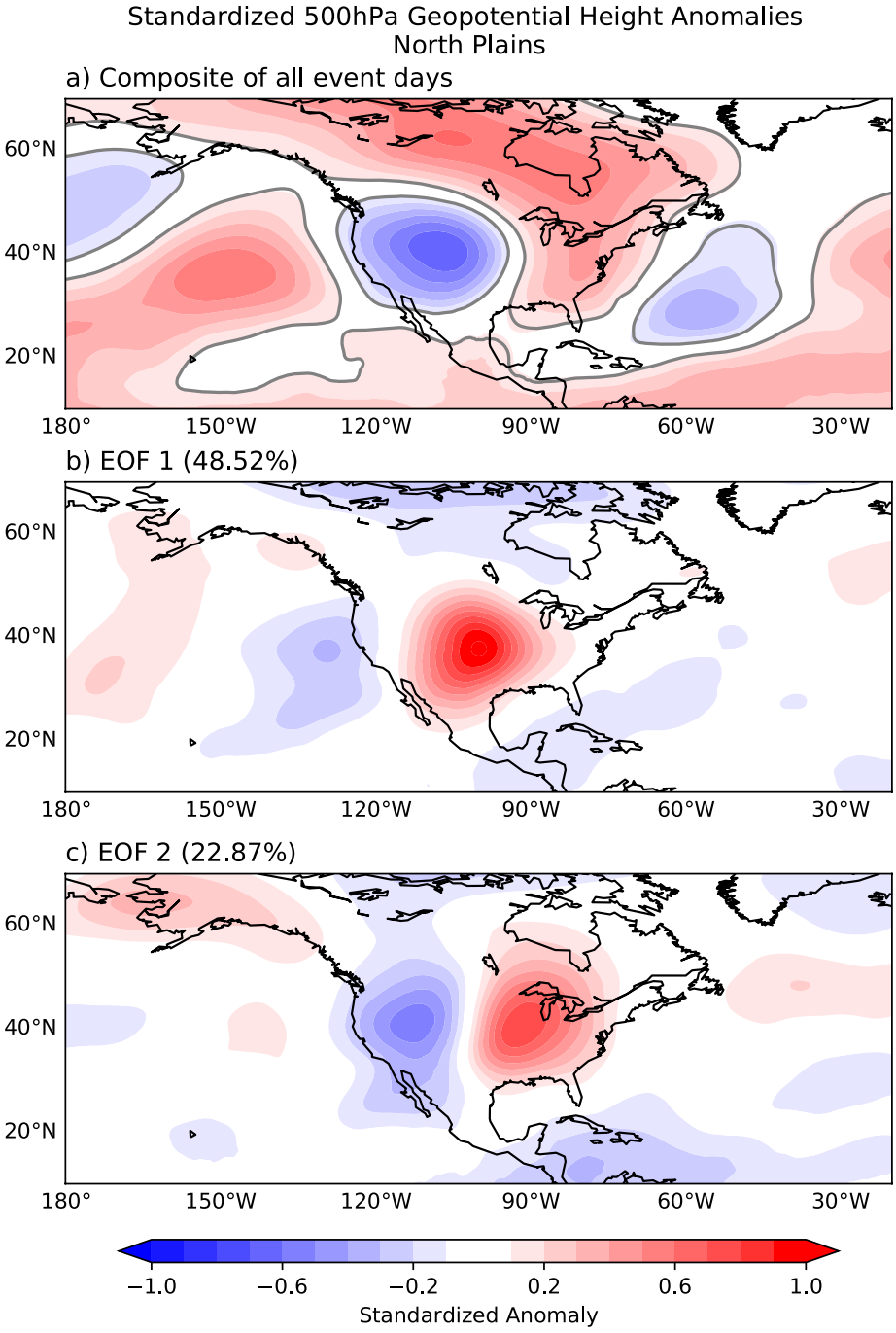


Figure 3.18: As in figure 3.3 but for the NP.

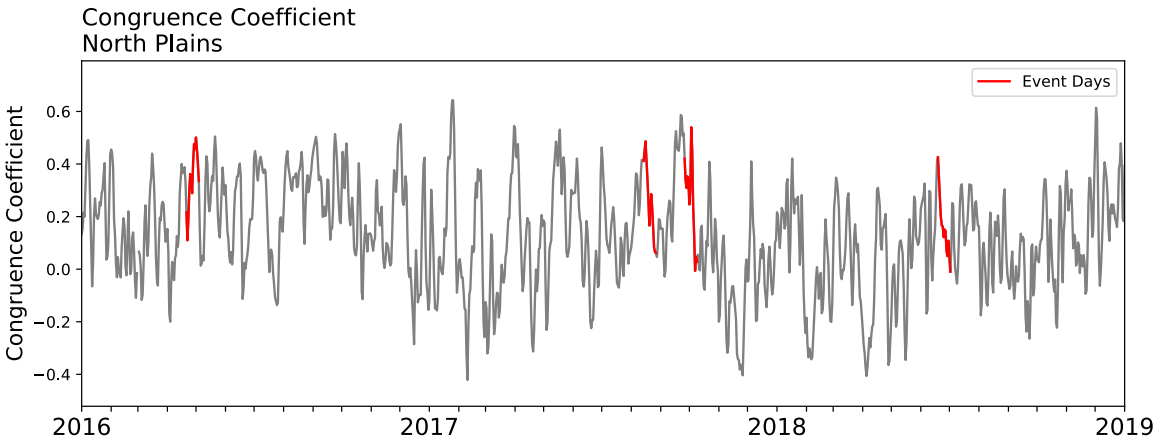


Figure 3.19: As in figure 3.4 but for the NP.

days from 1981-2018 we found that 34% of event days where above the threshold, and 6.7% of non-event days are above 0.35, Table 3.7. Although the NP has the highest frequency of days over the threshold with a POD of 34%, it also has the highest FAR of 92%. This is most likely due to the low number of events within the NP.

| | Event days | Non-Event days |
|---|---|---|
| Above Threshold | 80 | 908 |
| Below Threshold | 158 | 12724 |

Table 3.7: As in table 3.1 but for the NP.

The coupled patterns of geopotential height and precipitable water from the MCA are seen in Fig. 3.20. Unlike the other regions, the NP has an anomaly dipole within the height field that looks similar to the height composite, Fig. 3.18a. The ridge to the northeast of the region is much deeper in magnitude than the trough to the southwest of the region. The anomaly within the precipitable water field is aligned with the ridging seen in the height field. Unlike the previous regions, the MCA conducted on random days is slightly different than the MCA on our event days, Fig. A.11. The coupled patterns for random days is similar to other regions, with a large ridge

centered over the region, instead of a dipole, with a precipitable water anomaly in the same position. When analyzing the expansion coefficient time series, again, we see no distinct difference between the wet and the dry season events.

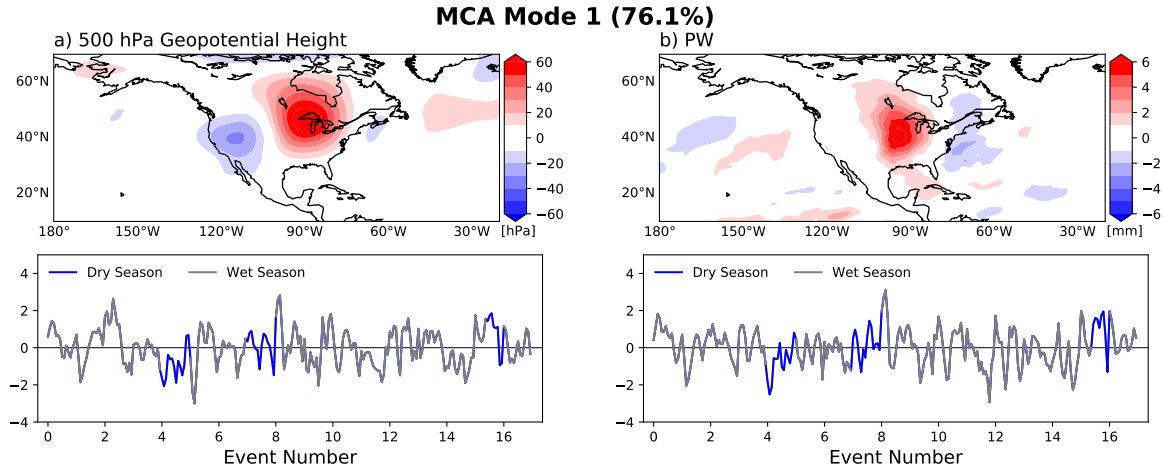


Figure 3.20: As in figure 3.5 but for the NP.

Using the height composites alone in the NP shows very little skill. Unfortunately, when using both heights and precipitable water composites this skill does not improve. The composite of precipitable water within our NP events is seen in Fig. 3.21. During our events we see a positive anomaly of precipitable water over northeast NP with a negative anomaly over the southwest NP. This pattern is different than the typical large positive anomaly over the entire region, found in most other regions. The contingency table of all event days during our time period while using the precipitable water and height composite is seen in Table 3.8. We found that the POD of NP events decreased to 19.7%, while the FAR stayed nearly constant at 91%. There were 492 days similar to our event patterns that are not associated with an event, while there were 191 event days that were not captured as events. Therefore, these patterns are not very skillful at predicting our event days within the NP.

| | Event days | Non-Event days |
|---|---|---|
| Above Threshold | 47 | 492 |
| Below Threshold | 191 | 13140 |

Table 3.8: As in table 3.2 but for the NP.

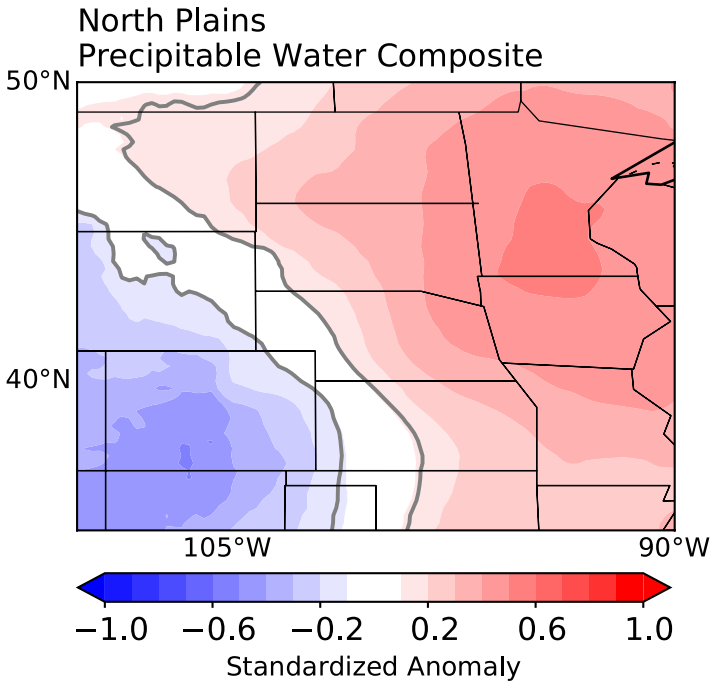


Figure 3.21: As in figure 3.6 but for the NP.

## 3.5 South Plains

The SP has a total of 57 events, which is the highest event count of all regions. There are only six years from 1981-2018 that the SP did not experience an event. Of particular interest is 2007, which had four events in the SP as well as two events in the NP. While much of the CONUS was in drought, both the SP and NP experienced above average precipitation throughout the year (NOAA-NCEI, 2008). Therefore, the only events that occurred during 2007 were in the Plains. Most of these events occur during the SP wet season, from April to October, seen in Fig. 3.22. There were only three events

seen during the dry season. The distribution of events is very similar to the NP, with three events occurring within the dry season and a maximum number of events in May and June, with 12 and 13 total events respectively.

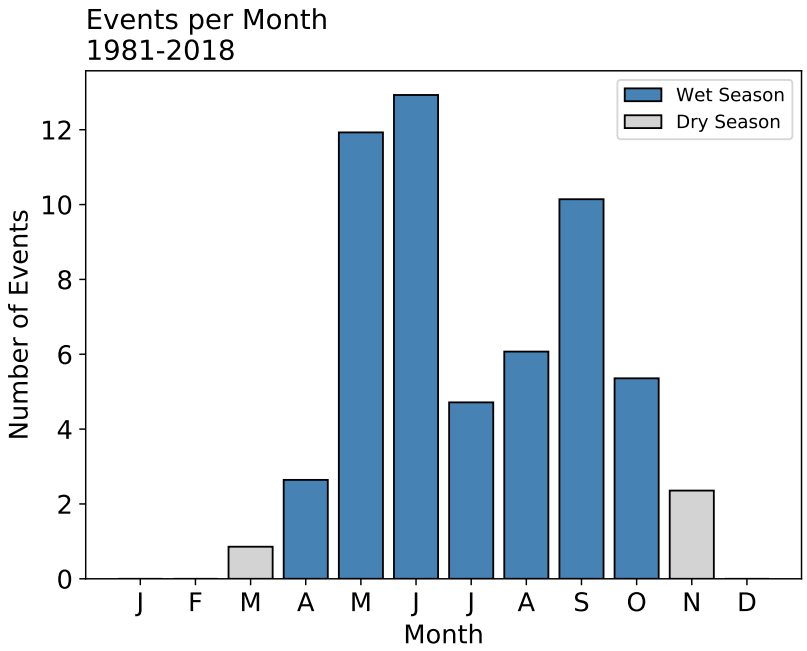


Figure 3.22: As in figure 3.2 but for the SP.

The composite of all event days geopotential height fields is seen in Fig. 3.23a. This composite has much lower overall magnitudes than any other regions composite. Yet, we still see the same trough-ridge dipole centered over the region. In contrast, the leading mode of event days, that explains 50.66% of variance, is a large anomaly spanning the entire southern CONUS, Fig. 3.25b. The second leading mode looks more similar to the composite with an anomaly dipole over the SP, Fig. 3.25c. These patterns are comparable to other regions modes, with a large signal over the region for the first mode and an anomaly dipole for the second mode.

In order to look at predictability within the SP, the time period of 2016 to 2018 was chosen due to the eight events that took place. The congruence coefficient time series

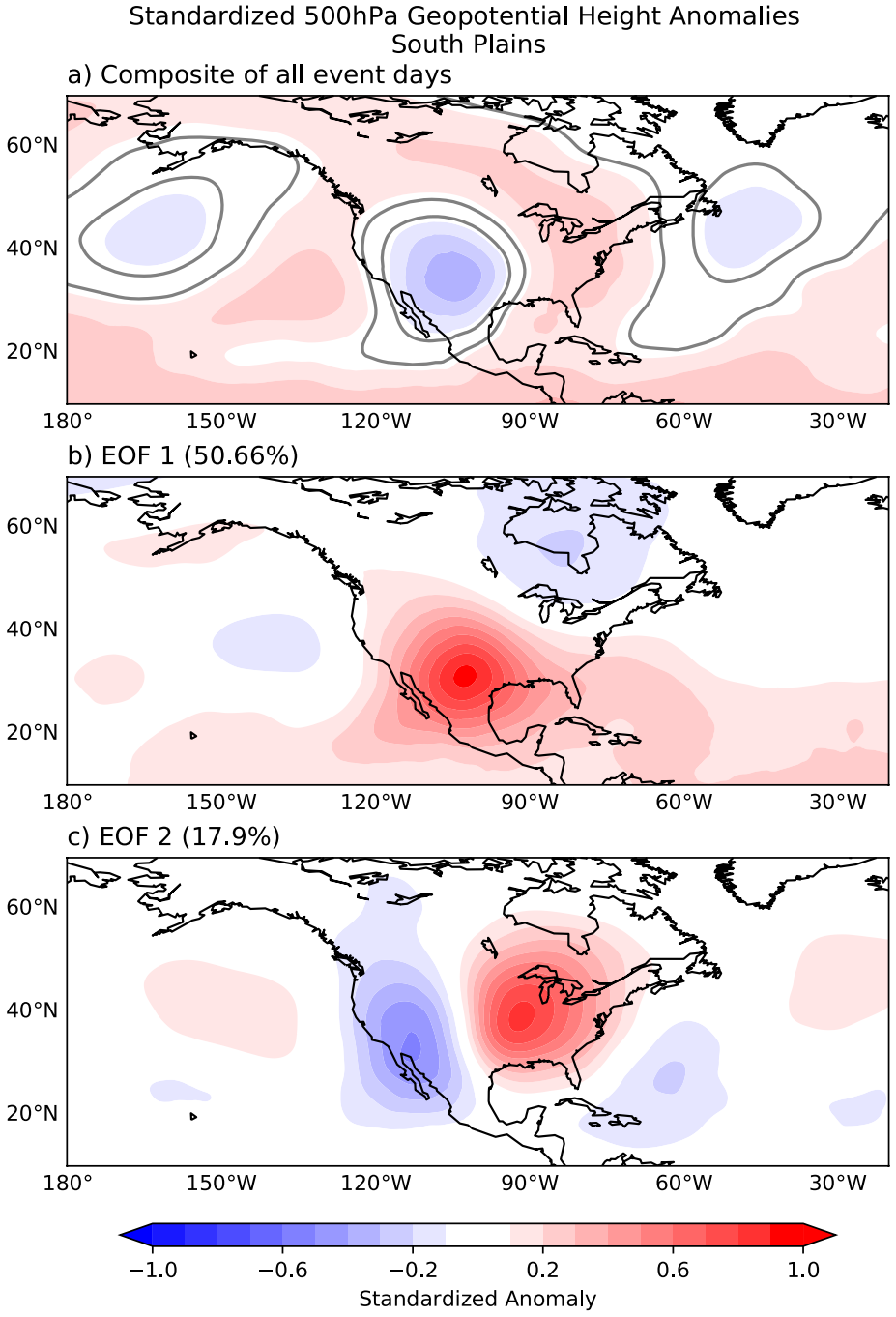


Figure 3.23: As in figure 3.3 but for the SP.

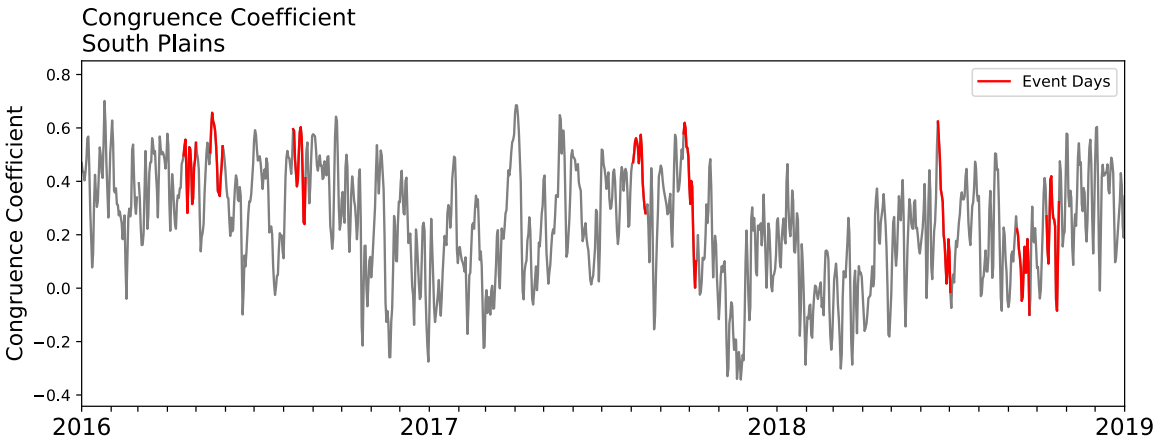


Figure 3.24: As in figure 3.4 but for the SP.

of 2016-2018 can be found in Fig. 3.24. All events in this time period are associated with days that have positive congruence coefficients, but there are no distinct signals during our events. For example, the first three events all have large coefficient values but are surrounded by many days that are non-event days with equally high values. This is also seen when analyzing all days congruence coefficient, Table 3.9. We see that 20% of event days and 9.5% of all non-events lie above 0.35. The FAR for the SP is 89%, with a total of 1238 false alarm days. There were also 638 event days that were missed by using 0.35 as a threshold, resulting in a POD of 20%.

| | Event days | Non-Event days |
|---|---|---|
| Above Threshold | 160 | 1238 |
| Below Threshold | 638 | 11834 |

Table 3.9: As in table 3.1 but for the SP.

Similar to other regions, we found that the SP leading mode for the MCA is large anomaly within the height fields with a well aligned precipitable water anomaly, Fig. 3.25. Yet, the location of the height anomaly is not seen centered over the region,

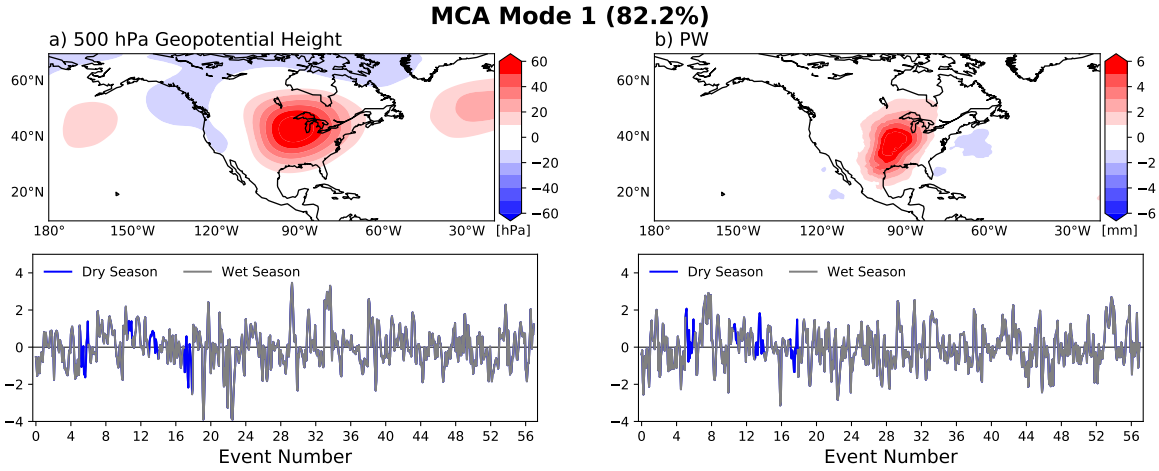


Figure 3.25: As in figure 3.5 but for the SP.

but instead centered within the GL, northeast of the region. Because there are so few dry season events, we cannot say if there are any differences between the expansion coefficient time series values between the two seasons.

Using the height composite alone to predict SP events resulted in the highest amount of false alarm days, 1238 days, for any region. However, when looking at predictability while using the composites of heights and precipitable water, this does improve. The precipitable water composite of SP events has significant precipitable water anomalies near the gulf and throughout most of the eastern portion of the SP, Fig. 3.26. Therefore, we want to find days with anomalous precipitable water throughout the region, with a similar height composite as Fig. 3.23a. Results are shown in a contingency table in Table 3.10. The previous 1238 false alarm days with heights alone, decreases to only 434 days with the addition of precipitable water. Yet, the FAR only decreases to 82% due to the low amount correct event days forecast. Using the patterns found from height and precipitable water during SP events shows very little skill in detecting our events days, with a POD of only 12%.

| | Event days | Non-Event days |
|---|---|---|
| Above Threshold | 98 | 434 |
| Below Threshold | 700 | 12638 |

Table 3.10: As in table 3.2 but for the SP.

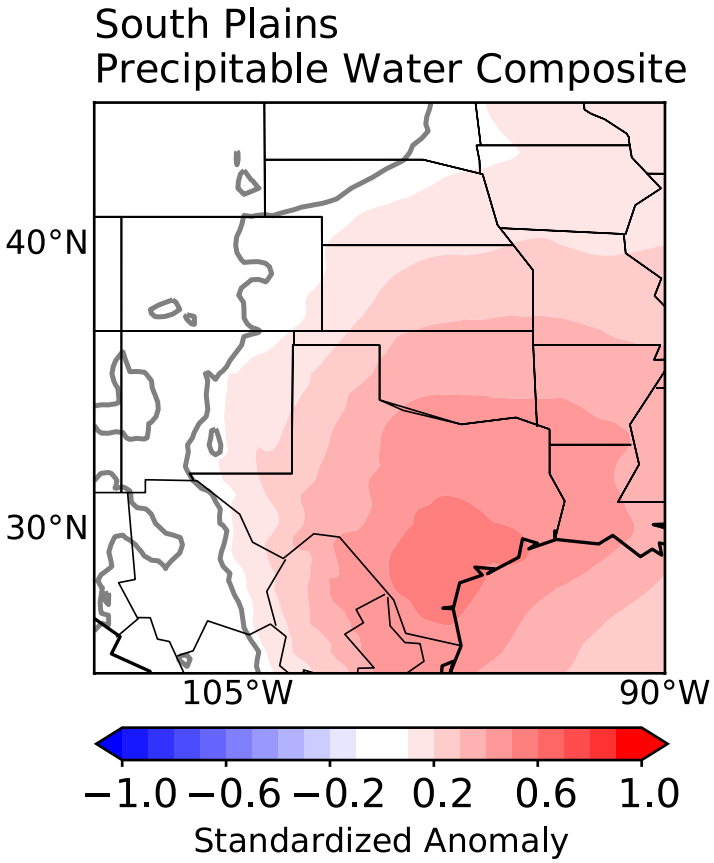


Figure 3.26: As in figure 3.6 but for the SP.

## 3.6 Mountain West

The MW experienced 50 events from 1981 to 2018, with more events at the beginning of the time period. For example, from 1981 to 1985 the MW had 13 events, or 25% of all MW events, seen in Fig. 3.1b. Due to the size of the MW region there two different wet seasons that were found when conducting the PCA on monthly average precipitation. West of the Rocky Mountains has a wet season similar to the WC, from

November to March. While, the east of the Rocky Mountains has a wet season more similar to the Plains from June to October. There are many more events that occur within the wet season of west MW, than in the east MW, as seen in Fig. 3.27. Also, we see that there were no events that occurred in April or August from 1981-2018.

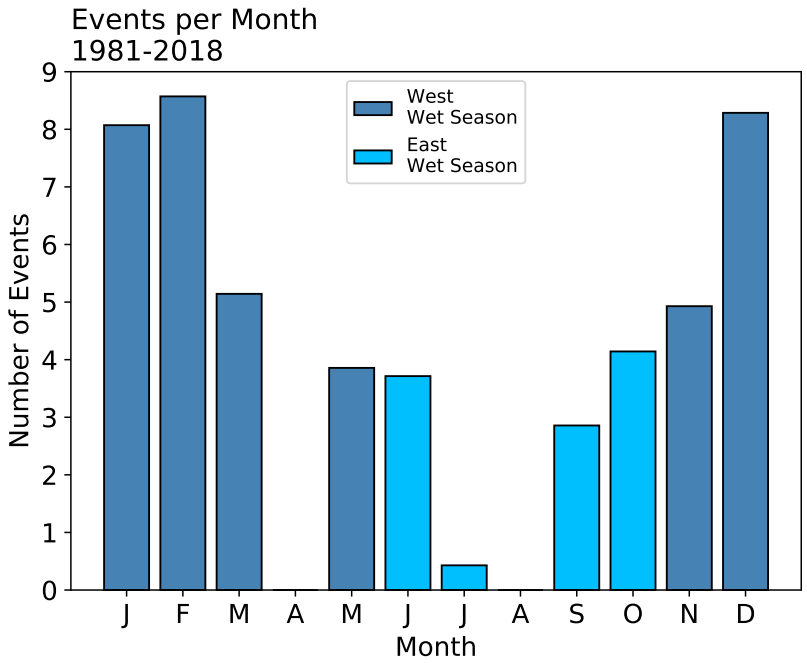


Figure 3.27: As in figure 3.2 but for the MW.

Similar to the SP, the MW event days height composite has relatively low standardized anomalies when compared to other regions, Fig. 3.28a. The pattern found has a trough-ridge pattern centered over the region with a negative anomaly to the north and a positive anomaly to the south. The leading mode from our PCA, Fig. 3.28b, shares the same large anomaly as other regions. This anomaly is centered to the left of the region with an anomaly of opposite sign found upstream and downstream. The anomaly upstream, in the North Pacific, has a larger magnitude than most secondary anomalies found in other regions leading mode. The second leading mode, explaining 20.26% of the variance, is a meridionally oriented anomaly dipole centered on the left

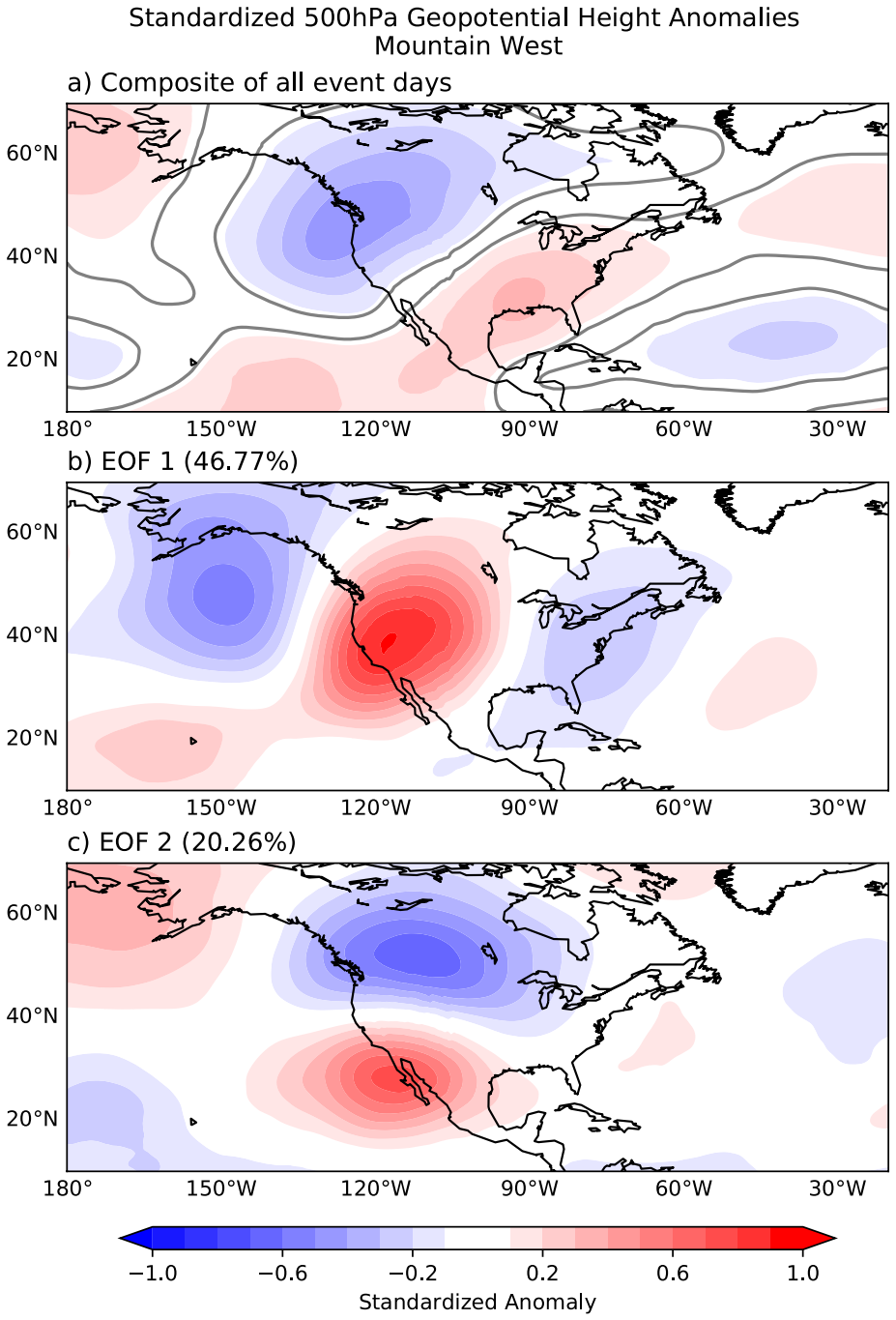


Figure 3.28: As in figure 3.3 but for the MW. Bars are colored based on the two separate wet seasons within the MW. The west MW wet season is in dark blue, while the east MW wet season is seen in light blue.

side of the region, Fig. 3.28c. Although this is similar to the composite, the exact placement and orientation of the anomaly dipole is quite different.

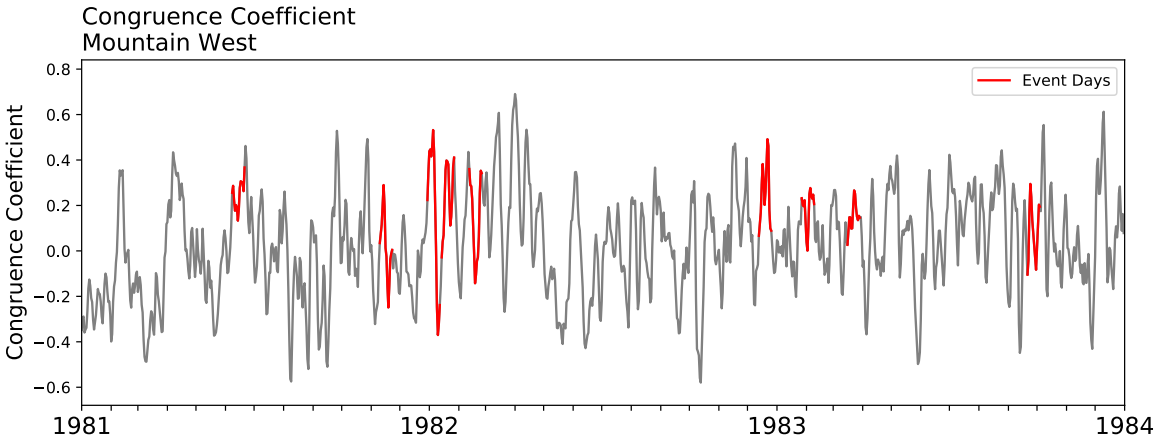


Figure 3.29: As in figure 3.4 but for the MW.

To illustrate predictability using our events height composite, an example time series of congruence coefficient from 1981-1983 is seen in Fig. 3.29, with 8 events seen in red. Some events are associated with local maximums, indicating that the event days are similar to our height composite. For example, the three events near the beginning of 1983 all have local maximums compared to the non-event days around them, but the event toward the end of 1983 is surrounded by days with large coefficients. This may be a result of the seasonality within the MW. To illustrate, the three events at the beginning of 1983 are within the wet season of West MW, while the event at the end of 1983 is within the wet season of East MW. Table 3.11 shows the number of days above or below a coefficient threshold of 0.35. We found that 19% of event days are above the threshold, while only 5.4% of non-event days are above the threshold. Yet, there are still 707 non-event days that have height patterns similar to our event composite without being considered an event, with a FAR of 84%. The POD of event days is quite low at 19%, with only 132 event days detected.

| | Event days | Non-Event days |
|---|---|---|
| Above Threshold | 132 | 707 |
| Below Threshold | 568 | 12463 |

Table 3.11: As in table 3.1 but for the MW.

The leading mode of the MCA of MW event day's 500 hPa height field and precipitable water fields are seen in Fig. 3.30, with their corresponding expansion coefficient time series. The leading mode explains 68.7% of the total covariance between the two fields. The height field found from the MCA, Fig. 3.30a, looks remarkably similar to the leading mode of our PCA, Fig. 3.28b. The only difference arises from the magnitude of the trough in the North Pacific, which could be due to the standardization of the height field in the PCA. We also see a precipitable water anomaly aligned with the large positive anomaly within the height field. The magnitude of the precipitable water anomaly is lower than any other regions, which is expected given the lower overall precipitation amounts in the MW.

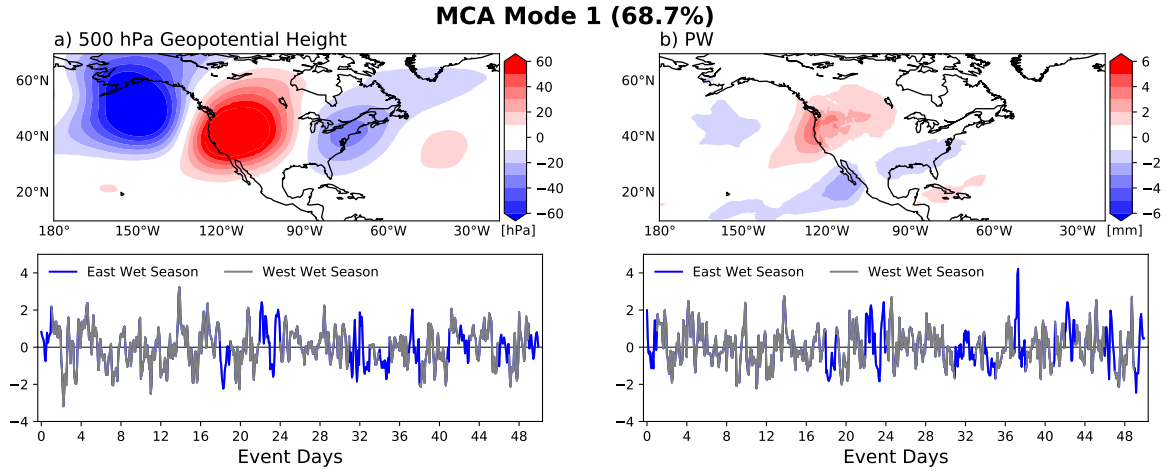


Figure 3.30: As in figure 3.5 but for the MW. The time series are labeled based on the two wet seasons found in the MW, east MW wet season (blue) and west MW (gray).

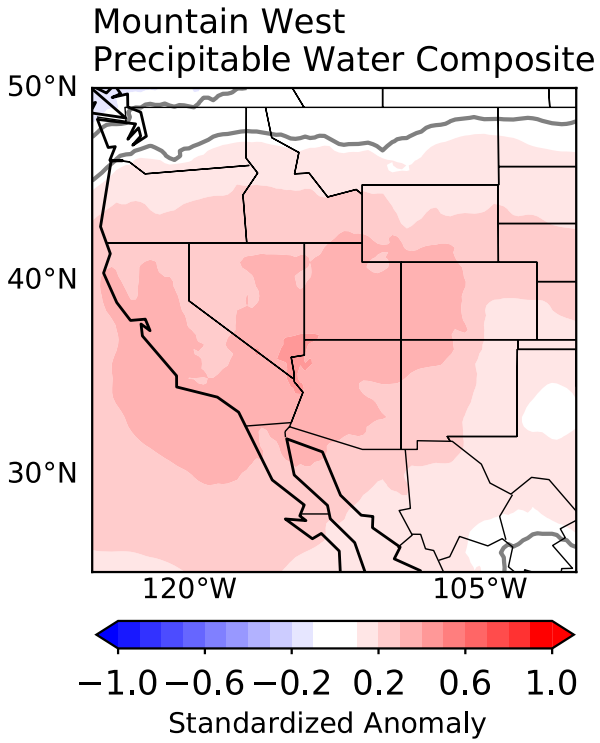


Figure 3.31: As in figure 3.6 but for the MW.

Similar to other regions, the addition of precipitable water helps to decrease the FAR and also decreases the POD. The composite of precipitable water used is seen in Fig. 3.31. During our events we see significant anomalous precipitable water throughout the entire region. The contingency table of all days during our time period while utilizing both precipitable water and height composites is seen in Table 3.12. The POD is shown to be only 9.6%, which is the lowest of all regions. While the FAR decreased from 84% with heights alone, to 77% with both, which is the lowest of all previous regions. The number of false alarm days decreases greatly from 707 days to only 227 days passing the threshold of 0.35 for both heights and precipitable water. Nevertheless, there are still 568 MW event days that are not detected when comparing event composites to all days.

| | Event days | Non-Event days |
|---|---|---|
| Above Threshold | 67 | 227 |
| Below Threshold | 633 | 12943 |

Table 3.12: As in table 3.2 but for the MW.

## 3.7 West Coast

The WC had 51 total events, with about one or two events occurring per year. There were only 7 years throughout 1981-2018 that did not experience an event in the WC. The WC also experiences the most events during the boreal winter (DJF) than any other region. This is due to a distinct wet season from October to April. All extreme events in the WC occur during the wet season, with no events occurring from March to September in our time period.

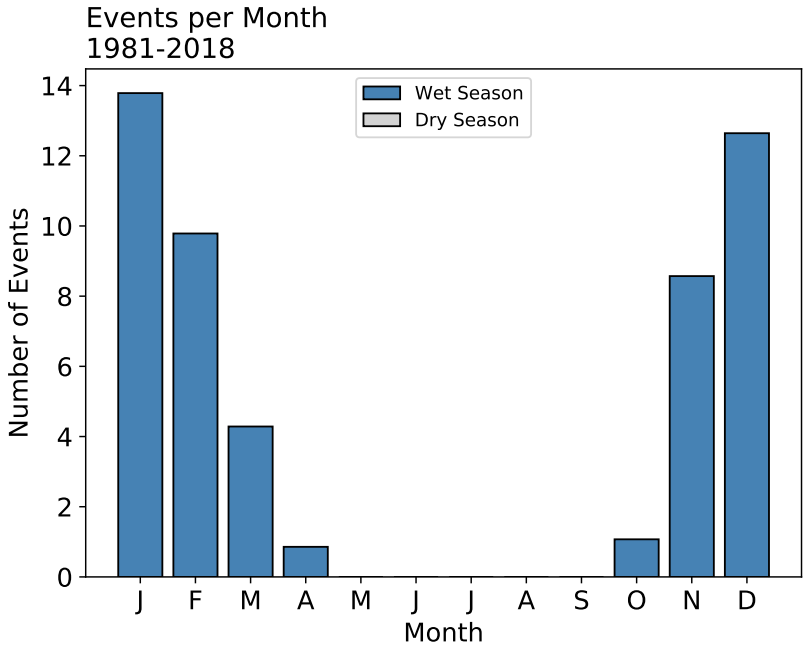


Figure 3.32: As in figure 3.2 but for the WC.

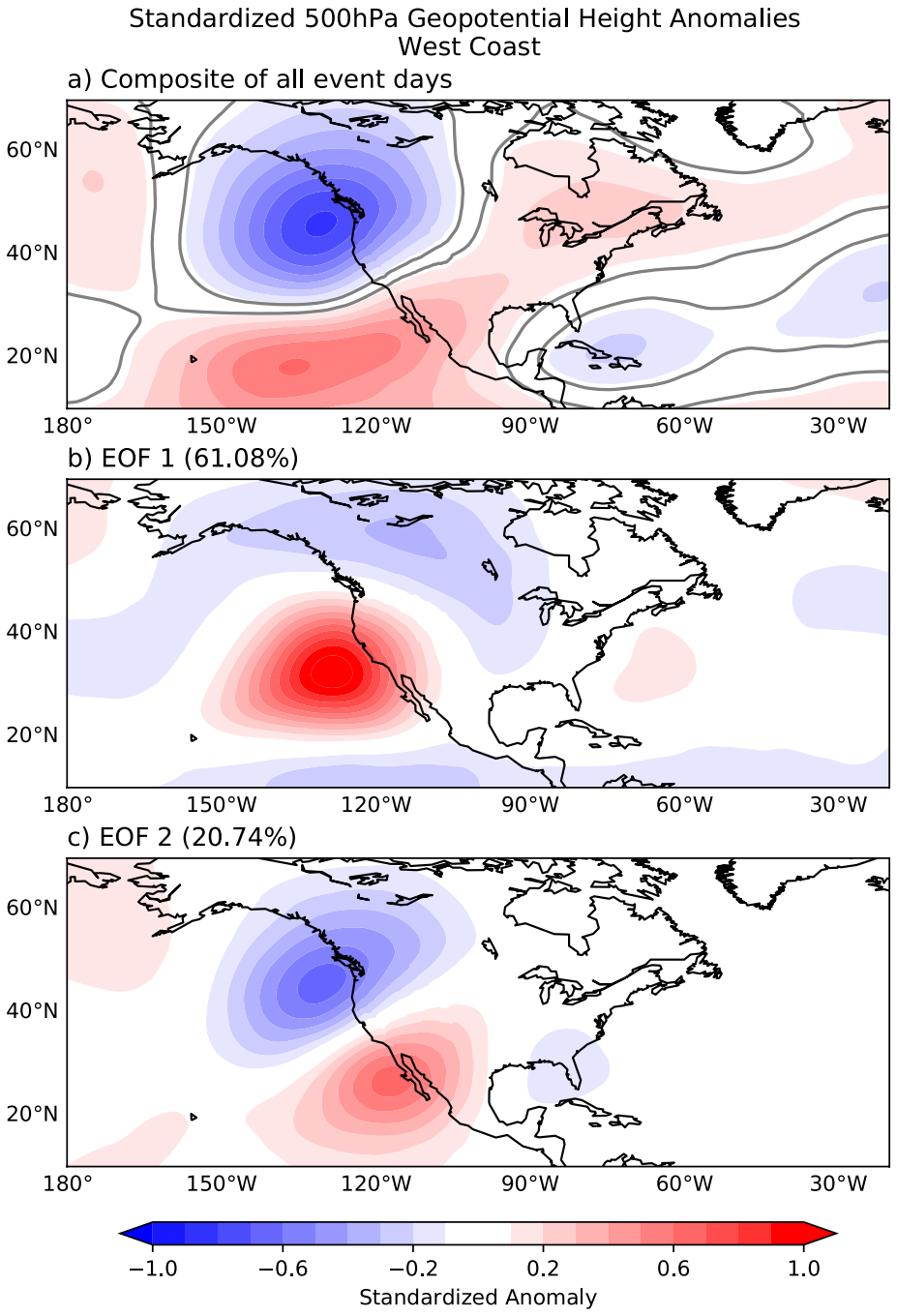


Figure 3.33: As in figure 3.3 but for the WC.

The composite of all event days within the WC is much different than any other region. Although it still has a anomaly dipole, it is oriented north/south in the eastern Pacific, Fig. 3.33a. The magnitude of the trough, to the north, is greater in magnitude of the ridge, to the south. This synoptic set up would allow for anomalous moisture flux from the Pacific into the region. The first two leading modes are similar to other regions, Fig. 3.33b/c. The leading mode explains 61% of the variance and is a large anomaly centered off the coast near the region. While the second mode, explaining 20.7% of the variance, is an anomaly dipole oriented meridionally centered in the same area as the first mode. This pattern looks similar to the composite of event days, but the center of the southern anomaly is much closer to the coast.

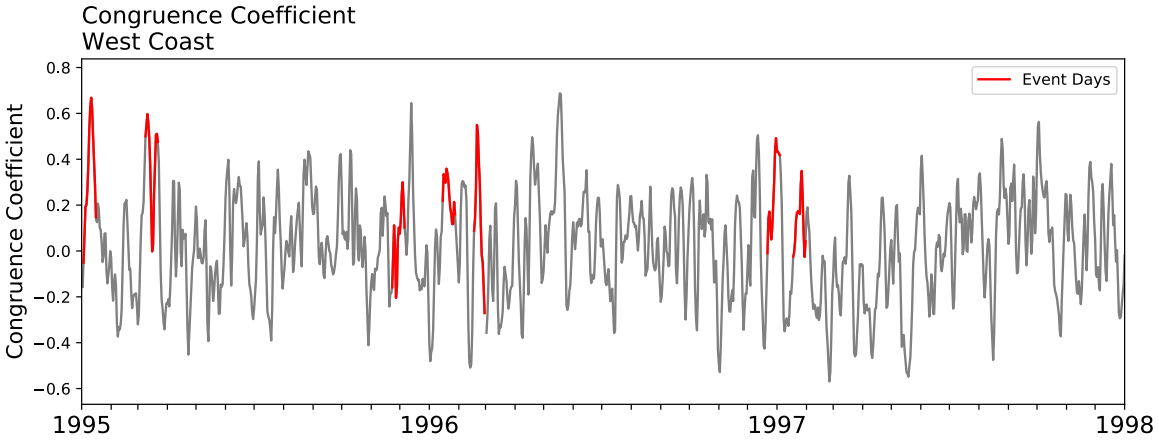


Figure 3.34: As in figure 3.4 but for the WC.

To look at predictability of WC events congruence coefficient for all days between 1995 and 1997 will be inspected, Fig. 3.34. During this time period there were 7 events that occurred. For the first two events in 1995 we see very large coefficient magnitudes, corresponding to local maximums. The other five events also have positive coefficients but have non-event days surrounding near the events with similar values. For the entire time period of 1981-2018 we see 30% of WC event days and 5.4% of non-event days

are over a coefficient value of 0.35, seen in table 3.34. Therefore, the POD for our events days is 30%. There were 714 false alarm days during the entire time period and 153 event days that were correctly detected, this results in a FAR of 77% which is the lowest of all regions when only using height composites.

| | Event days | Non-Event days |
|---|---|---|
| Above Threshold | 211 | 714 |
| Below Threshold | 502 | 12443 |

Table 3.13: As in table 3.1 but for the WC.

The leading mode of the coupled pattern between geopotential heights and precipitable water found using MCA of WC events explains 79.1% of the covariance. The height field shows a large ridge along the west coast with troughing occurring both downstream and upstream of the ridge. Once again, this large ridge is associated with a positive precipitable water anomaly. This positive anomaly is a part of an anomaly dipole off the west coast that is oriented southwest to northeast.

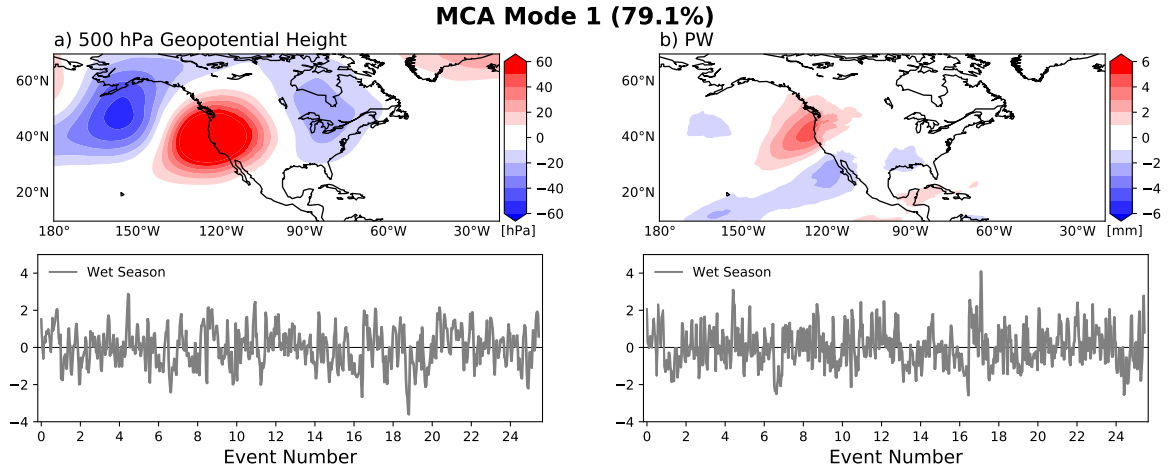


Figure 3.35: As in figure 3.5 but for the WC.

Using the height composite alone within the WC results in the lowest FAR of all regions. Therefore, we can expect to see an even lower FAR when utilizing both the height composite and the precipitable water composite, Fig. 3.36. Similar to other regions, the WC precipitable water composite is a large positive anomaly within the region. The contingency table for predictability of WC events using both height and precipitable water composites is seen in Table 3.14. We found that there are 153 event days that are accurately detected, while 560 event days are missed. This resulted in a lower POD of 21%. However, the number of false alarm days goes from 714 days when using height alone, to only 355 days when using both variables. Thus, the FAR decreases to 70% resulting in the lowest FAR with the highest POD of all regions.

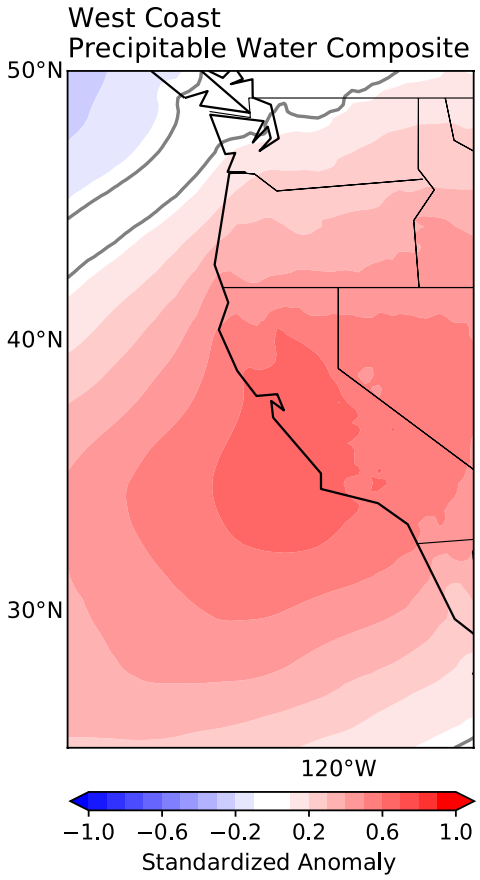


Figure 3.36: As in figure 3.6 but for the WC.

| | Event days | Non-Event days |
|---|---|---|
| Above Threshold | 153 | 355 |
| Below Threshold | 560 | 12802 |

Table 3.14: As in table 3.2 but for the WC.

## 3.8 Summary of Regions

All seven regions were found to have a trough/ridge dipole, with varying orientation, within their respective event day 500hPa height composites. These composites all could lead to rising motion under quasi-geostrophic theory that would help enable precipitation to occur. It was also shown that the first mode of variability found for the regions all had a dominant anomaly within the region of interest. This pattern is therefore likely non-physical and instead might be a result of propagating features during our event days. Predictability of regional extreme precipitation events is low when using a single predictor of 500hPa geopotential heights, seen by low POD values and high FAR values. When using two predictors, the composites of 500hPa geopotential height and precipitable water, POD decreases while FAR increases, seen in Table 3.15. The WC has the highest POD with two predictors with the lowest FAR, which are both good for predictability. This shows the WC might be more predictable using synoptic features than other regions. The NP has inflated values of POD and FAR compared to the other regions due to the lower amount of events within the region. Overall, the use of two predictors did result in an improvement with less false alarm days than with one predictor.

| | Heights Alone | | Heights and Prec. Water | |
|---|---|---|---|---|
| | POD | FAR | POD | FAR |
| NE | 20% | 89% | 13% | 88% |
| SE | 19% | 85% | 16% | 83% |
| GL | 30% | 84% | 22% | 78% |
| NP | 34% | 92% | 20% | 91% |
| SP | 20% | 89% | 12% | 82% |
| MW | 19% | 84% | 10% | 77% |
| WC | 30% | 77% | 21% | 70% |

Table 3.15: Summary of POD and FAR for using heights alone as a predictor as well as using heights and precipitable water together as a predictor for all seven regions.

# Chapter 4

# Extreme Precipitation Impacts

During the Pres2ip workshop hosted in the summer of 2018, stakeholders stressed the need to fully understand the impacts of extreme precipitation events. Although there might be an extreme amount of precipitation, it might not result in impacts on the ground. Therefore, impacts of these events need to be analyzed in order to be confident that the events we have found are impactful for the regions.

## 4.1 Tropical Cyclone Influence

It is well known that land falling Tropical cyclones (TCs) can cause a devastating amount of damage along the coast of the United States. This damage may be caused by a variety of sources, including the heavy precipitation that occurs during landfall (Klotzbach et al., 2018). The drivers of TCs are much different than that of mid-latitude precipitation. Therefore, it is important to examine the influence TCs may have in our events. Within the algorithm for defining our events, there are two steps that may help limit TC activity. The first being that we must have at least 5 rainfall days, or 3 for MW, over 10mm. After landfall many TCs weaken and may not produce enough rainfall to pass this rainfall day threshold. The second being that the heaviest rainfall day and the surrounding two days may not make up over 50% of the events precipitation. This eliminates short duration precipitation events that may occur due to land falling TCs.

In order to examine TC influence within our events the International Best Track Archive for Climate Stewardship (IBTrACS) was used to find all tropical cyclone activity within our events. Any extreme event day that had TC activity within the region is considered a TC affected day. It was found that there was only TC activity for the SP, SE and the NE. For each event with TC activity, the percent of total event rainfall that fell during the TC days was found. This gives an estimation of the influence of the precipitation from the TC for our events.

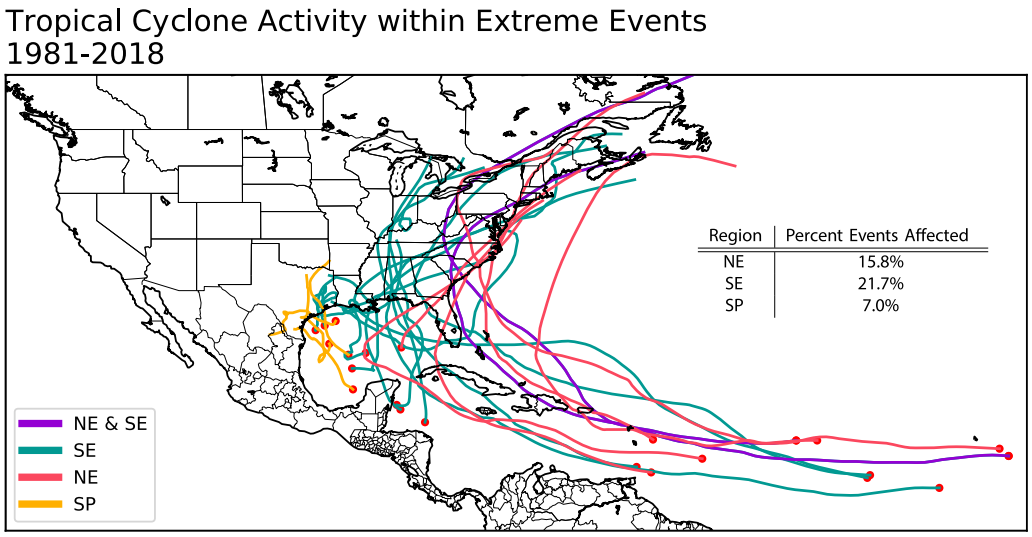


Figure 4.1: Tracks of tropical cyclones that occurred during our extreme events in the SP (yellow), SE (green), NE (orange) and the two cyclones seen in both SE and NE events (purple). Percent of events that have tropical cyclone activity within them can be seen in the table to the right.

All tracks of TCs that are seen within our events are seen in Fig. 4.1. The SE has the most TC activity within the events with 21.7% of all SE events have a TC in the region. However, only 15.8% of NE events and 7% of SP events are affected. The TCs all originated throughout the Atlantic Basin, with some originating in the Gulf and others further out into the Atlantic. Two of the TCs, Hurricane Chris in 1988 and Hurricane Hugo in 1989, were seen in an event within both the SE and NE. All TC

activity that was found is found in Table 4.1. There are some events within the NE and SE that have multiple TCs that occur during a singular event. For example, there is a SE event that started on August 28, 1988 that had 4 days of TC activity from Hurricane Chris and Hurricane Florence. These 4 days accounted for 34.8% of the total event rainfall. Therefore, the TC activity did provide a lot of the overall precipitation for this event. Seven of the ten events affected by TCs in the SE have TC days that make up 25% of the overall precipitation. While only three of the six events in the NE and three of four events in the SP make up 25% of the overall event precipitation.

Table 4.1: Tropical cyclone activity within extreme events within SE, NE and SP.

| | Event Start | Name | Days Affected | % Event Precip |
|---|---|---|---|---|
| **SE** | Oct 18, 1985 | Juan | 5 | 66.8% |
| | Aug 28, 1988 | Chris | 2 | 34.9% |
| | | Florence | 2 | |
| | June 25, 1989 | Allison | 4 | 18.7% |
| | Sept 19, 1989 | Hugo | 2 | 8.1% |
| | Aug 13, 1992 | Andrew | 4 | 6.1% |
| | June 3, 2001 | Allison | 9 | 68.0% |
| | Sept 5, 2004 | Frances | 4 | 62.6% |
| | | Ivan | 3 | |
| | May 30, 2005 | Arlene | 3 | 39.1% |
| | July 4, 2005 | Cindy | 3 | 26.3% |
| | | Dennis | 3 | |
| | May 15, 2018 | Alberto | 2 | 26.4% |
| **NE** | Aug 23, 1988 | Chris | 1 | 34.1% |
| | Sept 13, 1989 | Hugo | 1 | 0.5% |
| | Sept 4, 1996 | Fran | 5 | 42.6% |
| | | Hortense | 1 | |
| | Aug 9, 2004 | Bonnie | 2 | 9.6% |
| | | Charley | 1 | |
| | Aug 26, 2011 | Irene | 3 | 36.7% |
| | June 7, 2013 | Andrea | 2 | 10.6% |
| **SP** | June 11, 1993 | Arlene | 3 | 22.9% |
| | Sept 6, 1998 | Frances | 4 | 2.7% |
| | Sept 7, 2002 | Fay | 5 | 42.7% |
| | Aug 31, 2003 | Grace | 3 | 36.2% |

## 4.2 Impacts

Although direct impacts of our events may not be easily measured, we can instead look at typical storm reports. These storm reports can show us the typical precipitation type, possible storm characteristics and other impacts. Total storm reports for all NE events can be seen in Fig. 4.2a. The highest count for a single category in the NE is Thunderstorm Wind, reported when winds reach at least 50 knots or winds at any speed that produce damage within in a convective storm (Murphy, 2018). The next two highest are flood and flash-flood, which is indicative of impacts caused by flooding during the events. In Fig. 4.2b the total reports seen during the events for flash flood, flood and heavy rainfall were compared to totals for a 1000 random 14-day periods, or nonevents. There is a significantly different amount of reports in our events than in non-events for flash flood reports and flood reports. This confirms that the events are resulting in more impacts than typical 14-day periods. Other worthwhile reports seen during the events are hail, lightning and tornado which are all reporting during from convective storms. In Fig. 3.2, we see events that occur during the boreal winter (DJF). This may explain the winter storm, ice storm and winter weather reports seen in Fig. 4.2a. This suggests that impacts from these events may even occur during the regions typical dry season even though there are fewer overall events in the dry season.

Storm reports within our events in the SE vary greatly, seen in Fig. 4.3a. Similar to the NE, the SE has both convective storm reports (thunderstorm wind, tornado, hail and lightning) and winter storm reports (winter weather, winter storm, heavy snow and ice storm). This follows given our events happen throughout the year and therefore would create a vast range of impacts on the ground. Tropical storm reports also appear which suggests there is tropical storm activity during our events. When

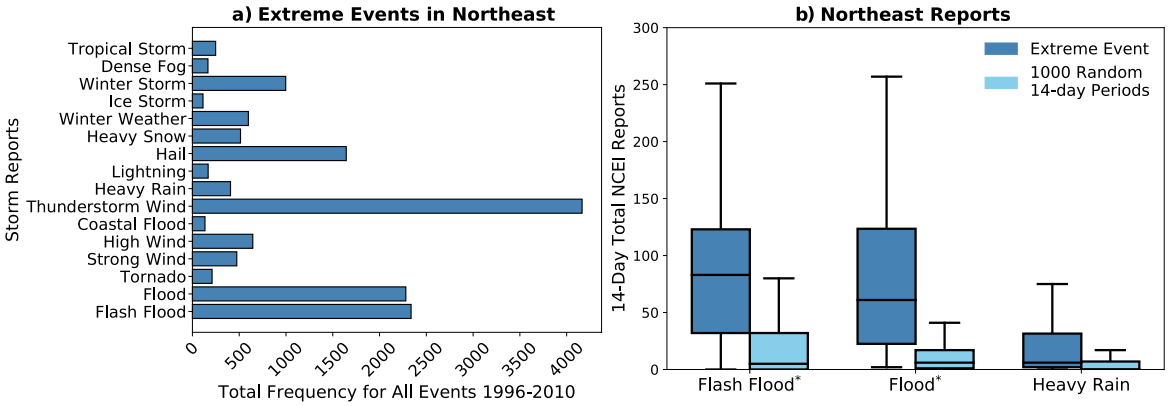


Figure 4.2: (a) All NCEI Storm reports from our extreme event days in the Northeast from 1996 to 2018. All reports that had less than 100 total counts are not shown. (b) Total NCEI Storm reports from 1996 to 2018 for Flash Flood, Flood and Heavy Rainfall for our extreme rainfall events in the Northeast, dark blue, and 1000 random 14-day periods excluding our extreme event days, light blue. Significant difference is found using a permutation test at p<0.1. Significance is indicated as a (*) next to the storm report labels, along the x-axis.

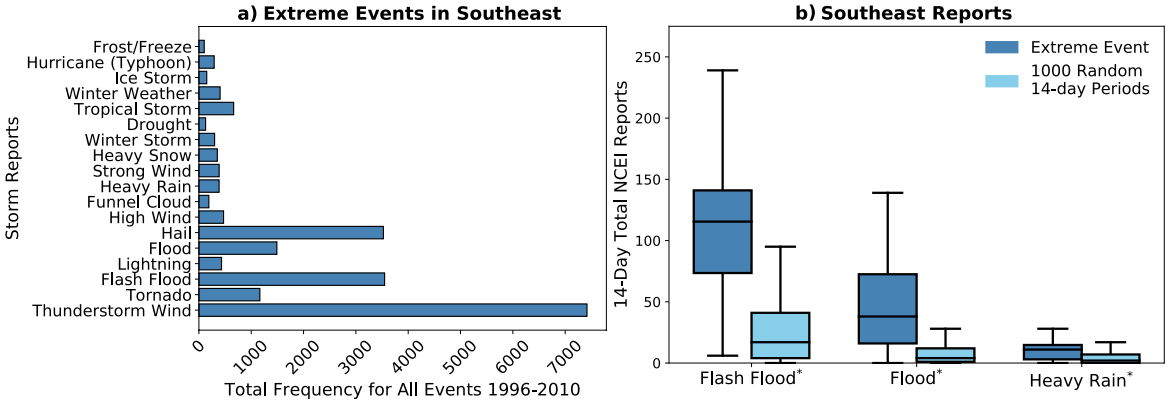


Figure 4.3: As in figure 4.2 but for the SE.

comparing our events to random 14 day periods we see a significant increase in the number of flash flood, flood and heavy rainfall in SE events, seen in Fig. 4.3b.

The GL region has the highest totals for storm report than all other regions, with a maximum of 14,000 reports of thunderstorm winds during the events. Storm reports during events within the GL correspond well with the timing of the events. Besides flood and flash flood, the highest totals for storm reports are seen for thunderstorm

wind, hail and tornado, seen in Fig. 4.4a. These are related to convective storm systems that normally occur during the warm season, or GL wet season. There are also a significant amount of storm reports for flash flood, flood and heavy rain during our extreme events, seen in Fig. 4.4b. The average flash flood count for GL events is near 120 reports for the 14-day period.

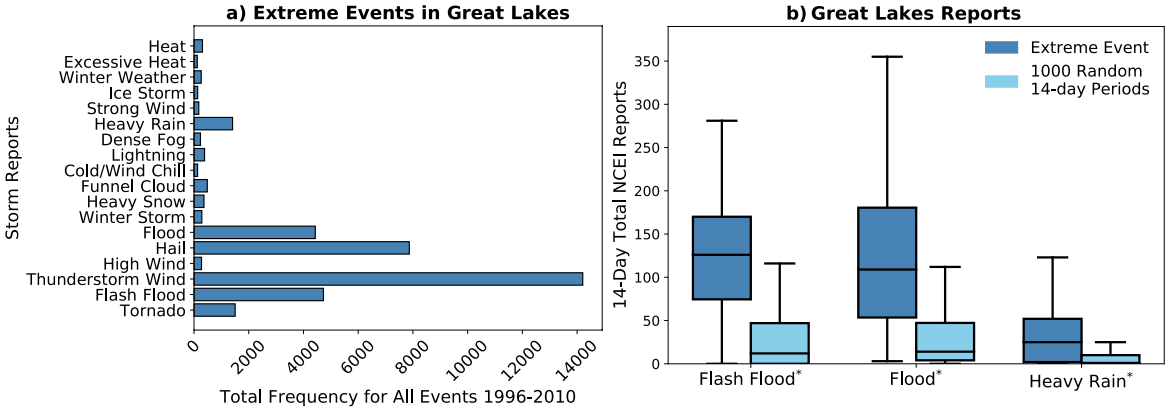


Figure 4.4: As in figure 4.2 but for the GL.

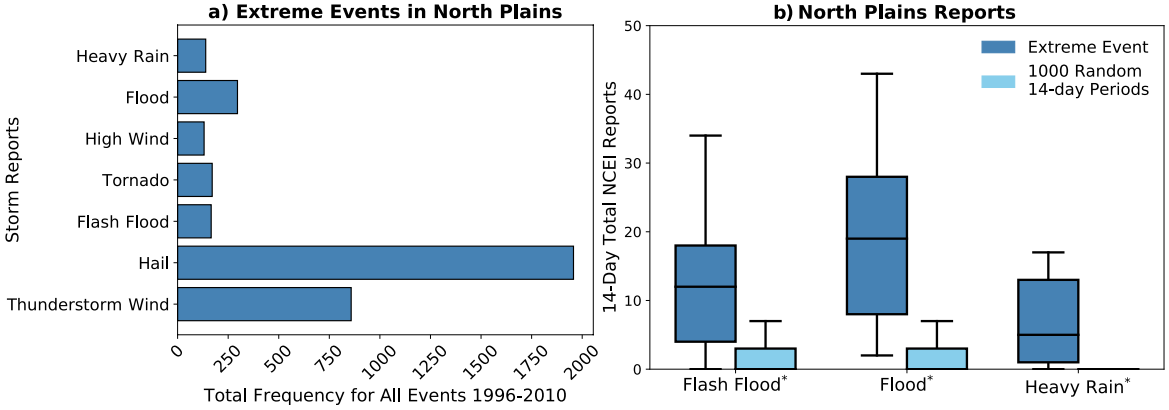


Figure 4.5: As in figure 4.2 but for the NP.

Within the NP, there are relatively few storm counts which is reasonable given there was only 17 events. Similar to previous regions, we see convective storm reports and rainfall reports, Fig. 4.5a. When comparing our NP events to non-events, we have a

significant amount of flash flood, flood and heavy rainfall reports during our events, Fig. 4.5b. When comparing the average number of reports of flash flood and flood for an event within the NP to any other region they are much lower. For example, NP events have an average of around 20 flood reports, whereas GL events have an average of around 100 reports. This is most likely a result of the size of the region because reports are made by county.

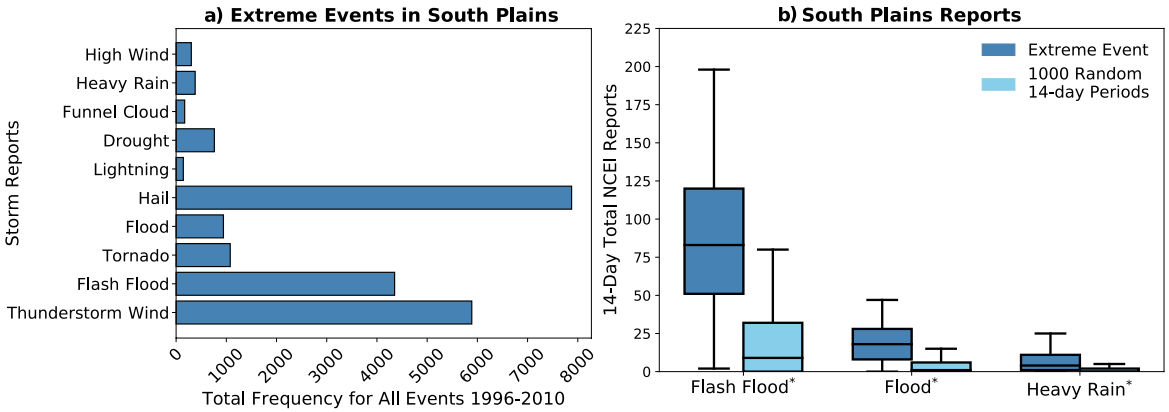


Figure 4.6: As in figure 4.2 but for the SP.

The southern plains is known for warm season mesoscale convective systems (MCS) producing large amounts of rainfall. In Fig. 4.6a, it is seen that events in the SP have many storm reports that are associated with convective systems, such as hail, thunderstorm wind, tornado and lightning. Given that most events within the SP occur during the warm season, it follows that convective reports are frequent during our events. Further, we see that we have a significant increase in reports of flash flood, flood and heavy rainfall during our events than non-event periods. The average number of flash flood reports for a SP event is over 75 reports, while the average for flood is less than 25 reports, Fig. 4.6b. This shows that events in the SP are more likely to produce large amounts of rainfall in a short amount of time, rather than rainfall that

would result in a report of a flood, despite the fact this precipitation is related to a 14-day event.

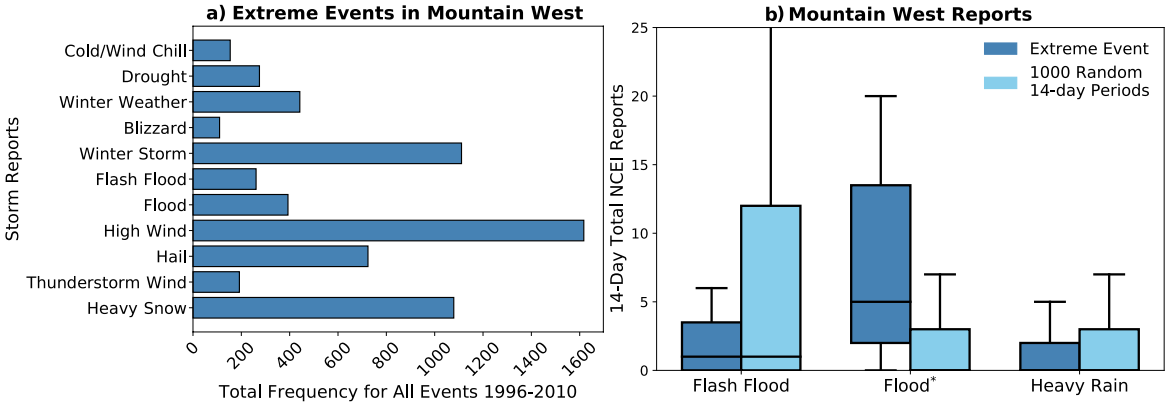


Figure 4.7: As in figure 4.2 but for the MW.

Due to large size of the MW, there are many different types of storm systems that might be responsible for the precipitation causing MW events. This is demonstrated by the variety of reports that resulted from the events, Fig. 4.7a. For example, there are reports that we would see from winter events, such as winter weather, blizzard, winter storm and heavy snow. As well as convective reports, such as hail and thunderstorm wind. Another interesting report that is seen is drought, which is contrary to an extreme precipitation event. This is most likely due to the fact that the entire MW does not need to receive extreme rainfall to be considered an event. For instance, one area of the MW might experience an event, while another area within the MW could be experiencing a drought. Given the two separate wet seasons that occur in the MW, this scenario could happen often.

When comparing precipitation reports during our events and random non-events we only see a significant number of flood reports. Given that we see many winter reports within MW events this most likely means that the MW experiences flooding from river

flooding and less short lived heavy rainfall that might result in a flash flood or heavy rain report.

As seen previously, all events in the WC occur during the cool season, therefore we can expect to see winter precipitation within our events. This is confirmed when examining the storm reports associated with our events, Fig. 4.8a. Along with the typical reports of flood, flash flood and heavy rain, we also see winter precipitation reports of winter storm and heavy snow. We found a significant difference between our event reports of flash flood, flood and heavy rain to non-events. The average number of flood report within a WC extreme events is near 20 reports in a single event. While average report counts for flash flood and heavy rainfall are below 10 reports, seen in Fig. 4.8b.

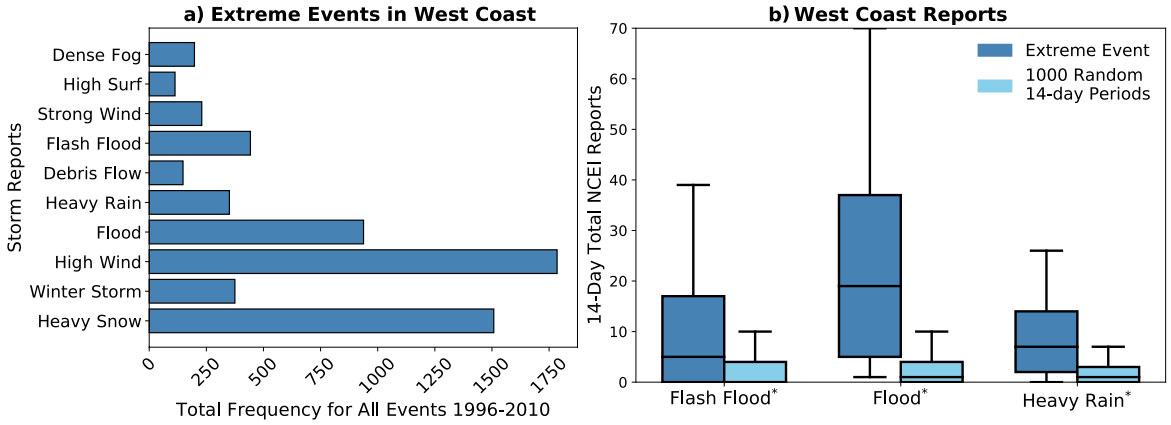


Figure 4.8: As in figure 4.2 but for the WC.

# Chapter 5

# Summary and Conclusions

In this study, we extended an existing database of 14-day extreme precipitation events created by Jennrich et al. (2020). We found that with the addition of 2010-2018 the overall monthly distribution of events does not change, while the yearly distribution shows an increased number of events at the end of the time period. By splitting the Great Plains into the SP and the NP, we found very few events in the NP and the highest number of events in the SP. This might be due to the area threshold used for the NP in the event classification algorithm, since, the NP is the smallest of all the regions, it would be more difficult for precipitation in the region to surpass this threshold. The typical timing of events is unique to each region. The NE, GL, NP and SP all have a wet season during the warm months; while the MW and WC have a wet season during the cool months. Whereas, the SE experiences precipitation throughout the entire year. Most regions experience the maximum number of events during their wet season, with the NE experienced the most events during its dry season.

Similarly to Jennrich et al. (2020), composites of all event days standardized 500hPa geopotential height anomalies from 1981-2018 showed a trough/ridge dipole that is oriented over the region. This synoptic set up is favorable for precipitation in a quasi-geostrophic framework. However, when finding the leading modes of the standardized height anomalies during our events we do not see this dipole. Instead we see a large anomaly centered over each region. While the second leading mode for each region is a dipole that is oriented either meridionally (WC, MW, NE and GL) or zonally (NP,

SP and SE). These patterns differ greatly from the respective regions composites and have similar patterns for every region. Therefore, the first leading mode shows the overall amplitude change of heights that occurs during our events, while the second shows an anomaly dipole that could be indicative of trough/ridge amplification that occurs during the events. Thus, predictability was based on the height composite of our event days. Every day's standardized 500hPa height anomaly fields from 1981-2018 was compared to the extreme events composite found for the region using congruence coefficient. Days above the congruence coefficient threshold of 0.35 were considered an event detection. We found that using heights alone results in very low skill of detecting our event days. All regions have a FAR of greater than 84% and the POD of all regions falls in between 19% to 34%. Therefore, there are many days within our events that have a height field that differs greatly from our event day composite even though Jennrich et al. (2020) showed significant anomalies. Although 500hPa geopotential heights may play a role in the formation of precipitation, heights alone are not a good predictor of extreme rainfall events. We see these patterns in, not only extreme precipitation days, but also in non-extreme days.

Coupled patterns of geopotential height and precipitable water were analyzed for all regions. This was done by using MCA on the covariance matrix of all event days height and precipitable water field. It was found that all regions had a similar leading mode with a large positive height anomaly centered over the region and an associated positive precipitable water anomaly. The patterns found in the height fields match very closely with the leading mode found when conducting the PCA on height days alone. When conducting the MCA on random, non-events the same leading mode emerges, with the exception of the NP. This indicates that the coupled patterns found in the event days MCA are not unique to our events, but instead large scale variability. Therefore, in order to look at predictability using both variable the composite of standardized heights

anomalies and standardized precipitable water will be used. Both fields must pass a congruence coefficient threshold of 0.35 to be considered a hit. We found that with the addition of precipitable water the POD decreases to a range of 12% to 22%, while the FAR decreases to a range of 70% to 91%. The WC and MW had the largest decrease in FAR with the addition of precipitable water. The WC also has the largest POD and lowest FAR, which indicates that the WC may be more synoptically driven than other regions. Overall, the addition of precipitable water does help to decrease the number of false alarm days, but also decrease the amount of event days that are detected. Again, this shows that although there is variability during the event, compositing alone will not find this variability. In order to have accurate predictions for decision makers to plan for these events, this variability must be understood to lower the false alarm days and increase accurately found event days.

In order to find large scale patterns associated with S2S extreme precipitation events, we want to understand the influence TC activity in our events. The only regions that have TC activity within their events are the SP, SE and the NE. It was found that overall, TC activity within the SP is minimal with only 4 total events affected. There is a larger influence of TCs within the SE and NE where 21.7% and 15.8%, respectively, of events are have TC activity. There were two SE events that actually have more than 50% of the event rainfall occurring during TC days. TC activity in events is important to understand, not only to help isolate patterns associated with mid-latitude precipitation, but also to find possible impacts of our events.

During our workshop hosted in June 2018, decision makers stressed that when defining an extreme event, impacts must be analyzed. Although direct economical impacts of our events can not be found, we instead can learn more about the typical storm reports seen within our events. Reports showed a wide variety of storm impacts

throughout all of the regions. Within the NE, SE, GL, NP SP and MW we see convective style storm reports such as hail, lightning and thunderstorm wind. All of these reports may result in impacts that may affect the region. While NE, GL, MW and WC all have winter weather storm reports. All regions have a significant number of flood reports when compared to random non-events. Miller et al. (2008) found that flooding is the costliest natural disaster. Therefore, our events may lead to devastating impacts on the ground without proper time to prepare and make decision to mitigate the risks.

Within this study we use regional division to find extreme precipitation events within seven regions. Because latitude and longitude boxes where made this may limit the number of events we find. If an event occurs that happens to lie over a regional division it may not be seen as an event due to its reduced size. This also creates "hot spots" for events within the center of our regions as seen in Fig 5.1. We also see difference in number of events that occur on the regional boundaries. For example, the west side of the SP has an average around 15 events per grid point but on the opposite of the SP/MW boundary the MW has an average of around 4 events. Going forward, finding these events without regional boundaries would help to find the events that do not perfectly fit within these seven regions.

Into the future, there is still much to learn about potential predictability of these events. Although, geopotential heights and moisture are a good foundation for predictability there are many more atmospheric variables to take into account. For example, 200 hPa zonal winds, moisture flux, sea surface temperature, soil moisture and evaporation could be analyzed in a similar fashion in order to find other important drivers of S2S extreme precipitation events that may happen before or during our events. In this study we focused on 14-day events, yet Jennrich et al. (2020) created a database of 30-day events as well. Therefore, a similar study could investigate

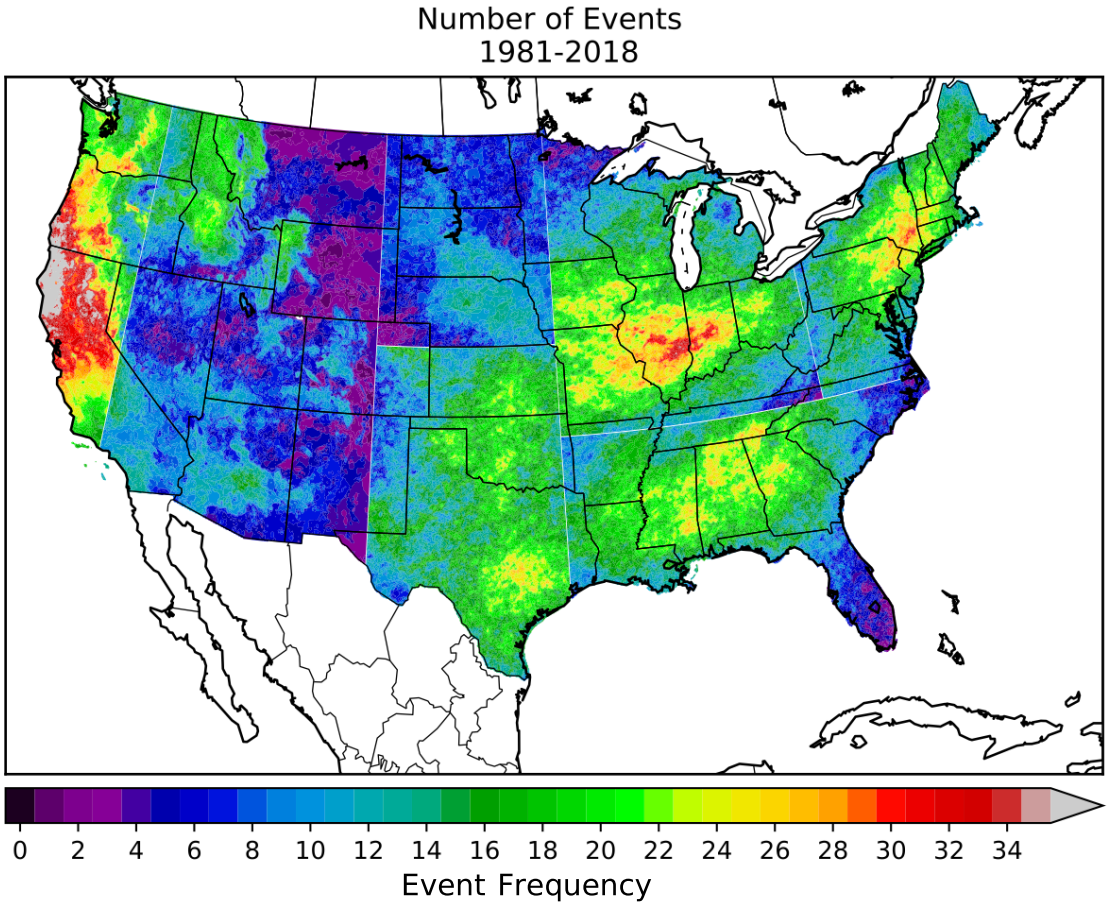


Figure 5.1: Event count at each grid point for all seven regions.

the potential predictability and impacts of longer events as well. Investigating these events within seasonal models could also revel important characteristics about how these events may or may not be forecast to occur. For example, if the same synoptic conditions found in our events in observations can lead to extreme precipitation in the models. Finally, finding direct economical impacts of our events could help decision makers understand the best way to create a more resilient population against extreme precipitation events.

# Reference List


Barlow, M., and Coauthors, 2019: North American Extreme Precipitation Events and Related Large-scale Meteorological Patterns: a Review of Statistical Methods, Dynamics, Modeling, and Trends. *Climate Dynamics*, **53 (11)**, 6835–6875, URL https://doi.org/10.1007/s00382-019-04958-z.

Bluestein, H. B., 1992: Synoptic-Dynamic Meteorology in Midlatitudes: Volume 1, Principles of Kinematics and Dynamics.

Bretherton, C. S., C. Smith, and J. M. Wallace, 1992: An intercomparison of methods for finding coupled patterns in climate data. *Journal of Climate*, **5 (6)**, 541–560, doi:10.1175/1520-0442(1992)005⟨0541:AIOMFF⟩2.0.CO;2.

Brunet, G., and Coauthors, 2010: Collaboration of the Weather and Climate Communities to Advance Subseasonal-to-Seasonal Prediction. *Bulletin of the American Meteorological Society*, **91 (10)**, 1397–1406, doi:10.1175/2010BAMS3013.1.

Copernicus Climate Change Service (C3S), 2017: ERA5: Fifth generation of ECMWF atmospheric reanalyses of the global climate. *Copernicus Climate Change Service Climate Data Store (CDS)*.

Curriero, F. C., J. A. Patz, J. B. Rose, and S. Lele, 2001: The association between extreme precipitation and waterborne disease outbreaks in the united states, 1948–1994. *American Journal of Public Health*, **91 (8)**, 1194–1199.

Cwik, P., E. R. Martin, R. A. Mc Pherson, H. Lazrus, J. C. Furtado, E. Mullens, C. M. Kuster, and M. J. Wagner, 2020: User's Perspective and Decision-Making Process Based on S2S Extreme Precipitation Forecast Products — What We Learned during the PRES2iP Workshop, URL https://ams.confex.com/ams/2020Annual/webprogram/Paper369119.html, AMS Annual Meeting.

Daly, C., M. Halbleib, J. I. Smith, W. P. Gibson, M. K. Doggett, G. H. Taylor, J. Curtis, and P. P. Pasteris, 2008: Physiographically Sensitive Mapping of Climatological Temperature and Precipitation across the Conterminous United States. *International Journal of Climatology*, **28 (15)**, 2031–2064.

Dong, L., L. Leung, J. Lu, and F. Song, 2019: Mechanisms for an Amplified Precipitation Seasonal Cycle in the U.S. West Coast under Global Warming. *Journal of Climate*, **32**, doi:10.1175/JCLI-D-19-0093.1.

Flanagan, P. X., J. B. Basara, J. C. Furtado, and X. Xiao, 2018: Primary Atmospheric Drivers of Pluvial Years in the United States Great Plains. *Journal of Hydrometeorology*, **19 (4)**, 643–658, doi:10.1175/JHM-D-17-0148.1.

Furl, C., H. Sharif, J. W. Zeitler, A. E. Hassan, and J. Joseph, 2018: Hydrometeorology of the Catastrophic Blanco River Flood in South Texas, May 2015. *Journal of Hydrology: Regional Studies*, **15**, 90 – 104.

Groisman, P. Y., R. W. Knight, and T. R. Karl, 2012: Changes in Intense Precipitation over the Central United States. *Journal of Hydrometeorology*, **13 (1)**, 47–66.

Hendrickson, A. E., and P. O. White, 1964: Promax: A Quick Method for Rotation to Oblique Simple Structure. *The British Journal of Statistical Psychology*, **17 (1)**, 65–70.

IPCC, 2012: *Managing the Risks of Extreme Events and Disasters to Advance Climate Change Adaptation*.

Jennrich, G. C., J. C. Furtado, J. B. Basara, and E. R. Martin, 2020: Synoptic Characteristics of 14-Day Extreme Precipitation Events across the United States. *Journal of Climate*, **33 (15)**, 6423–6440, doi:10.1175/JCLI-D-19-0563.1.

Karl, T. R., and R. W. Knight, 1998: Secular Trends of Precipitation Amount, Frequency, and Intensity in the United States. *Bulletin of the American Meteorological Society*, **79 (2)**, 231–242.

Klotzbach, P. J., S. G. Bowen, J. Pielke, Roger, and M. Bell, 2018: Continental U.S. Hurricane Landfall Frequency and Associated Damage: Observations and Future Risks. *Bulletin of the American Meteorological Society*, **99 (7)**, 1359–1376.

Kunkel, K. E., K. Andsager, and D. R. Easterling, 1999: Long-Term Trends in Extreme Precipitation Events over the Conterminous United States and Canada. *Journal of Climate*, **12 (8)**, 2515–2527.

Kunkel, K. E., S. A. Changnon, and J. R. Angel, 1994: Climatic Aspects of the 1993 Upper Mississippi River Basin Flood. *Bulletin of the American Meteorological Society*, **75 (5)**, 811–822.

Livneh, B., E. Rosnberg, C. Lin, B. Nijssen, V. Mishra, K. Andreadis, E. Maurer, and D. Lettenmaier, 2013: A Long-Term Hydrologically Based Dataset of Land Surface Fluxes and States for the Conterminous United States: Update and Extensions. *Journal of Climate*, **26**, 9384–9392.

Miller, S., R. Muir-Wood, and A. Boissonnade, 2008: *An Exploration of Trends in Normalized Weather-Related Catastrophe Losses*, 225–247. Cambridge University Press, doi:10.1017/CBO9780511535840.015.

Murphy, J. D., 2018: *National Weather Service Instruction 10-1605: Storm Data Preparation*. URL https://www.nws.noaa.gov/directives/sym/pd01016005curr.pdf.

NOAA-NCEI, 2008: State of the Climate: National Climate Report for Annual 2007. URL https://www.ncdc.noaa.gov/sotc/national/200713, accessed: 2020-10-19.

NOAA-NCEI, 2011: State of the Climate: National Climate Report for Annual 2011. URL https://www.ncdc.noaa.gov/sotc/national/201113, accessed: 2020-10-19.

NOAA-NCEI, 2019: U.S. Billion-Dollar Weather and Climate Disasters. URL https://www.ncdc.noaa.gov/billions/.

NOAA-NCEI, 2020: Storm Events Database. URL https://www.ncdc.noaa.gov/stormevents/.

North, G. R., T. L. Bell, R. F. Cahalan, and F. J. Moeng, 01 Jul. 1982: Sampling errors in the estimation of empirical orthogonal functions. *Monthly Weather Review*, **110 (7)**, 699 – 706, doi:10.1175/1520-0493(1982)110⟨0699:SEITEO⟩2.0.CO;2, URL https://journals.ametsoc.org/view/journals/mwre/110/7/1520-0493_1982_110_0699_seiteo_2_0_co_2.xml.

PRISM Climate Group, Oregon State University, 2004: URL http://prism.oregonstate.edu.

Richman, M. B., 1986: Rotation of Principal Components. *Journal of Climatology*, **6 (3)**, 293–335.

Robertson, A. W., A. Kumar, M. Peña, and F. Vitart, 2015: Improving and Promoting Subseasonal to Seasonal Prediction. *Bulletin of the American Meteorological Society*, **96 (3)**, ES49–ES53.

Schumacher, R. S., and R. H. Johnson, 2006: Characteristics of U.S. Extreme Rain Events during 1999–2003. *Weather and Forecasting*, **21 (1)**, 69–85.

Slater, L. J., and G. Villarini, 2016: "recent trends in u.s. flood risk". *Geophysical Research Letters*, **43 (24)**, 12,428–12,436, doi:10.1002/2016GL071199.

UN, 2015: *The human cost of weather-related disasters 1995-2015*. 1–30 pp.

Vitart, F., and Coauthors, 2017: The Subseasonal to Seasonal (S2S) Prediction Project Database. *Bulletin of the American Meteorological Society*, **98 (1)**, 163–173, doi:10.1175/BAMS-D-16-0017.1.

Zhao, S., Y. Deng, and R. X. Black, 2017: A Dynamical and Statistical Characterization of U.S. Extreme Precipitation Events and Their Associated Large-Scale Meteorological Patterns. *Journal of Climate*, **30 (4)**, 1307–1326.

# 1 Appendix A

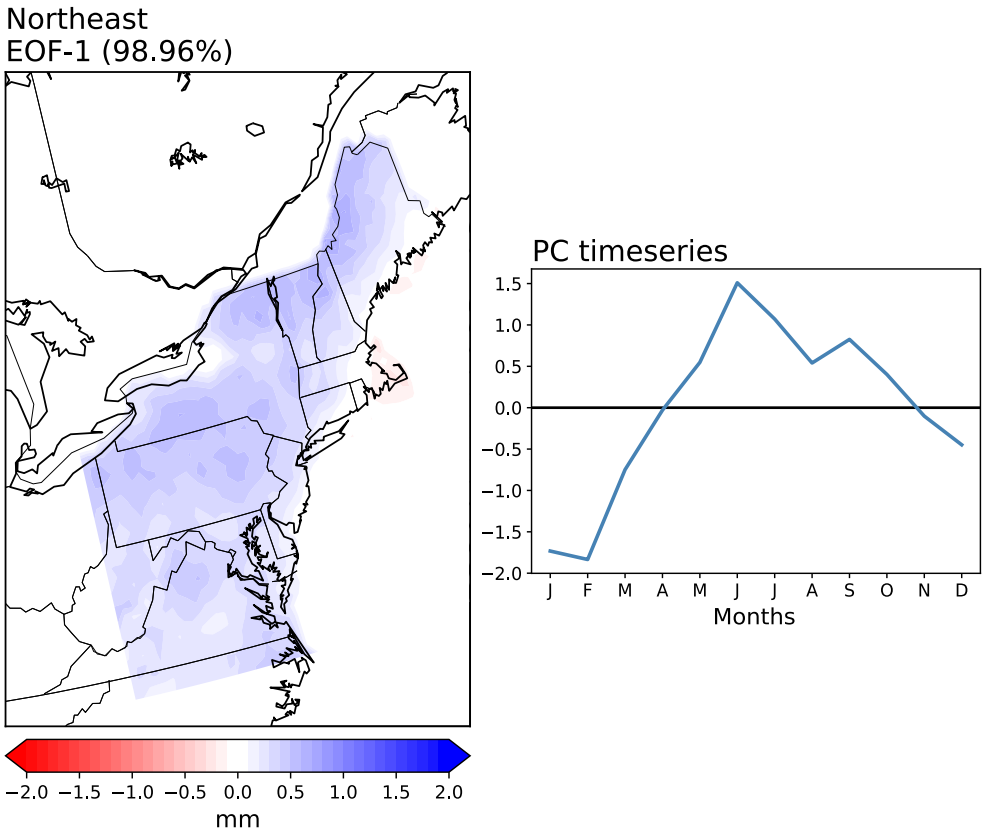


Figure A.1: The first mode of average monthly precipitation anomalies within the NE is seen to the left, with the corresponding PC time series to the right.

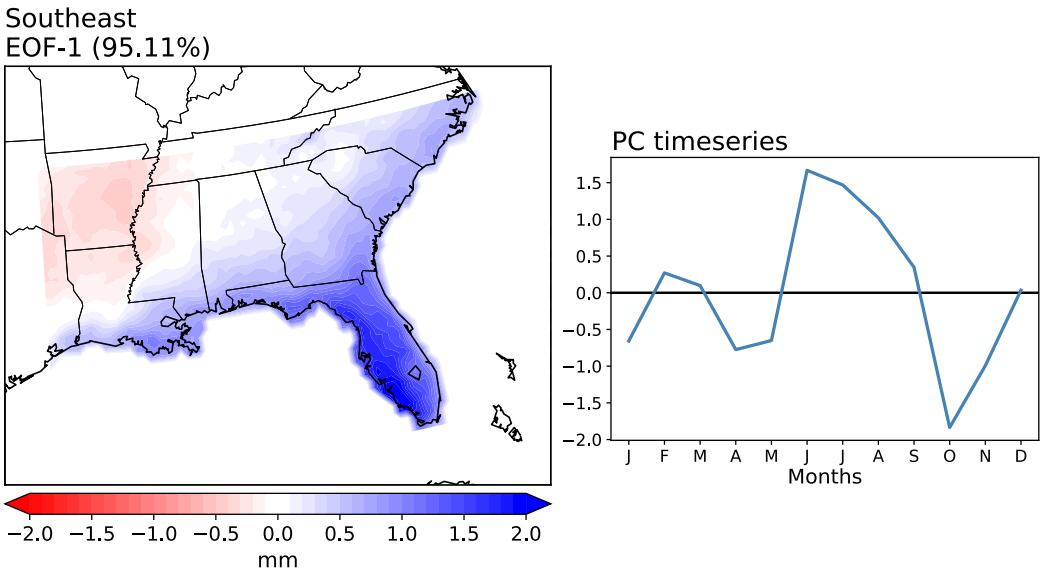


Figure A.2: As in Fig. A.1 but for the SE.

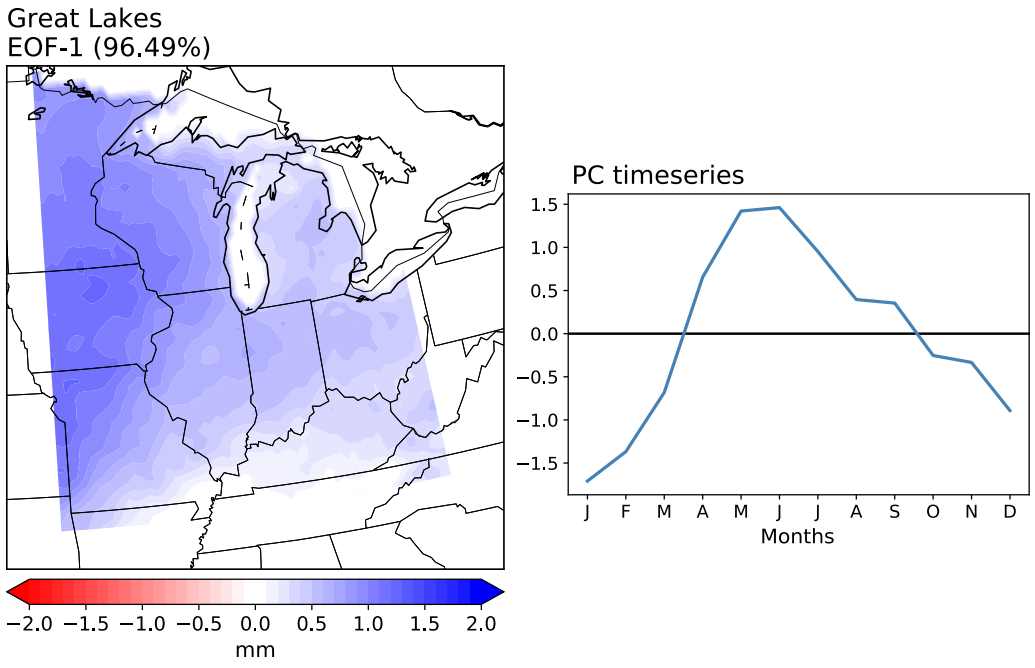


Figure A.3: As in Fig. A.1 but for the GL.

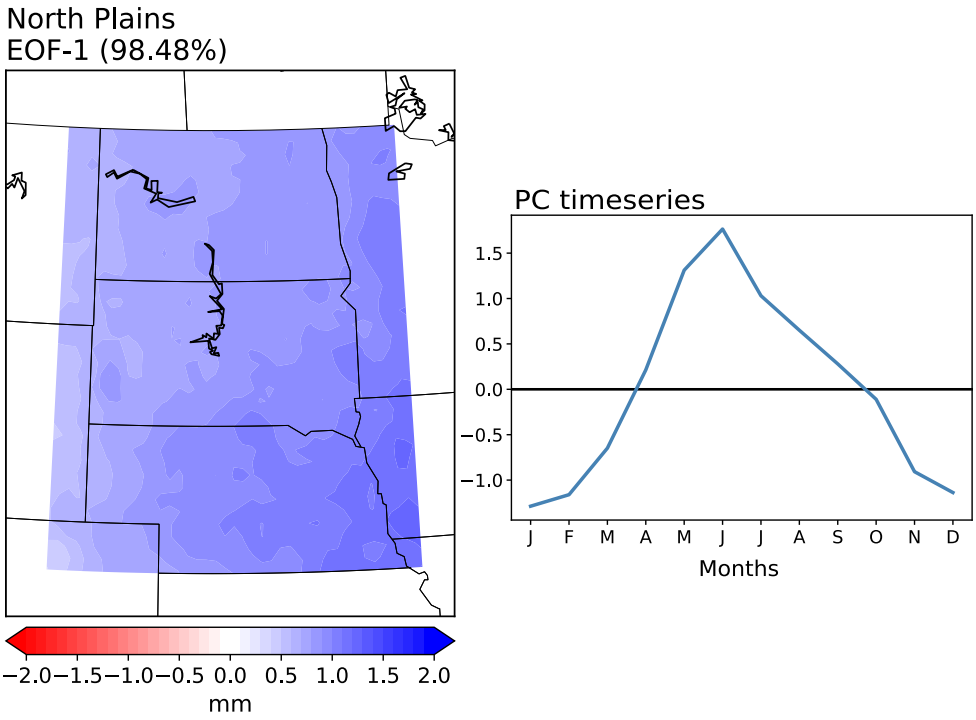


Figure A.4: As in Fig. A.1 but for the NP.

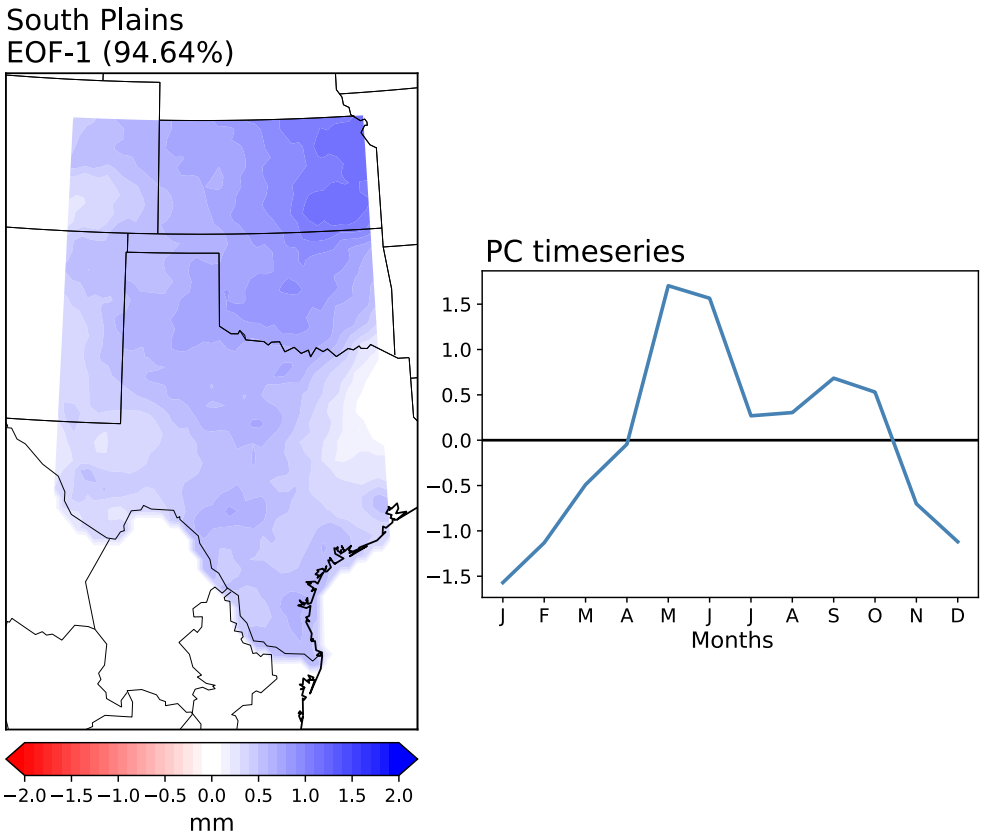


Figure A.5: As in Fig. A.1 but for the SP.

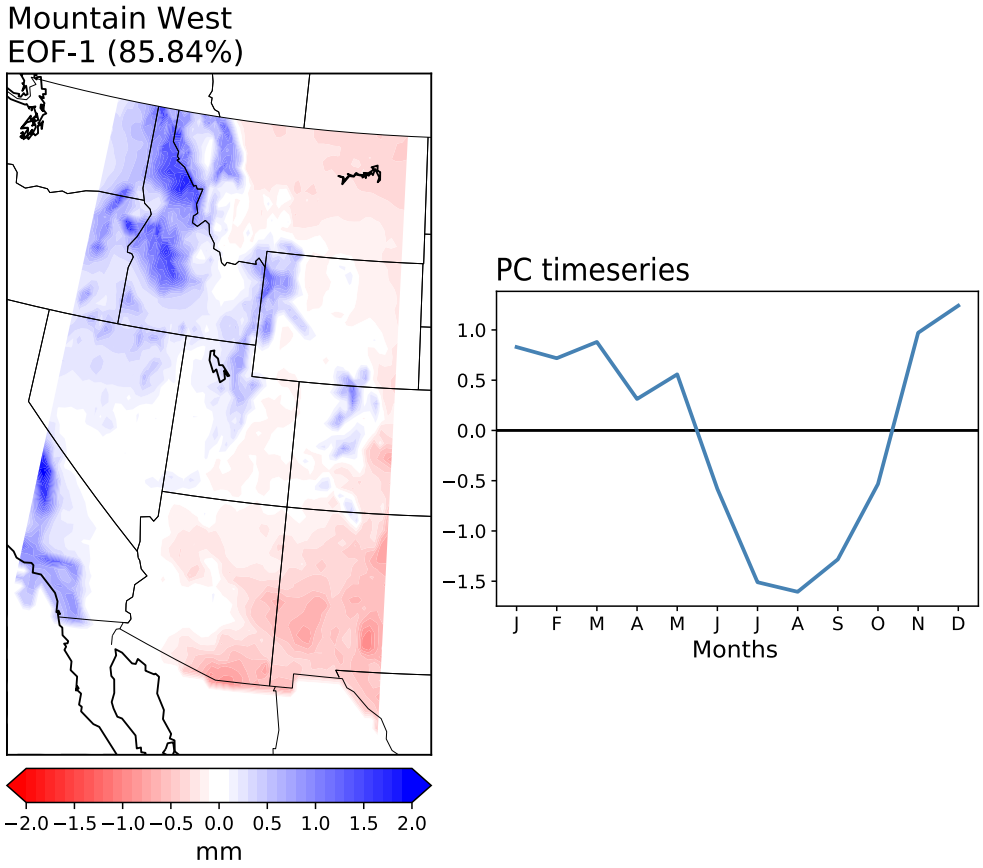


Figure A.6: As in Fig. A.1 but for the MW.

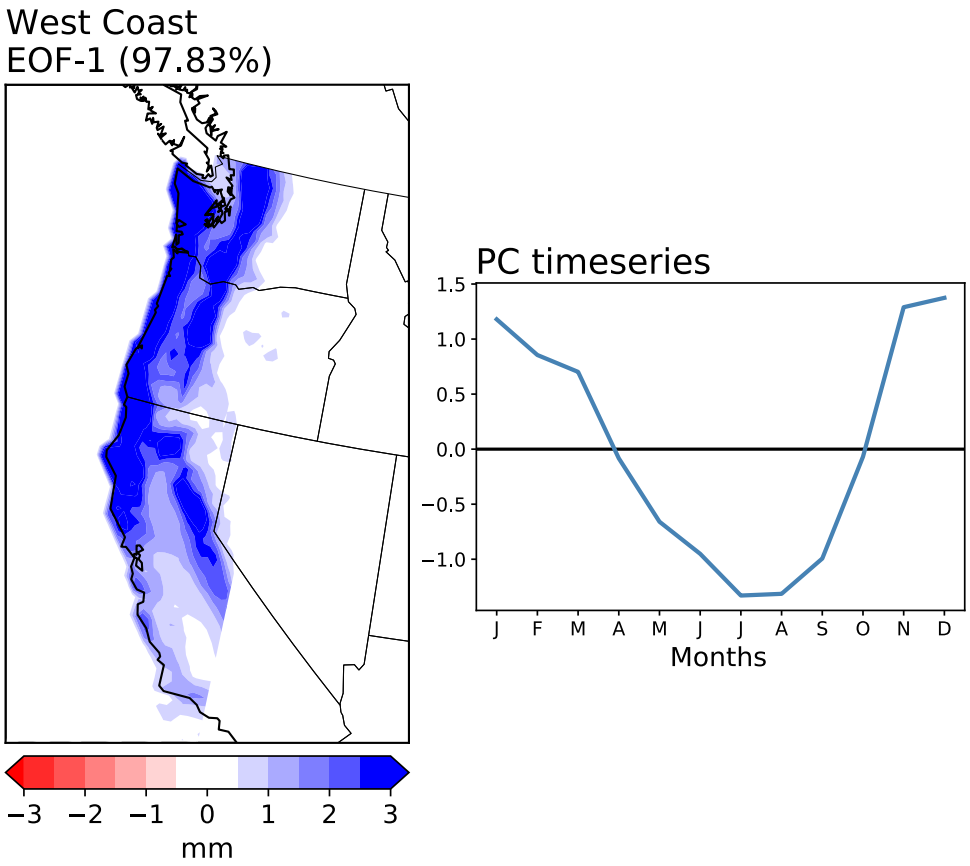


Figure A.7: As in Fig. A.1 but for the WC.

# 2 Appendix B

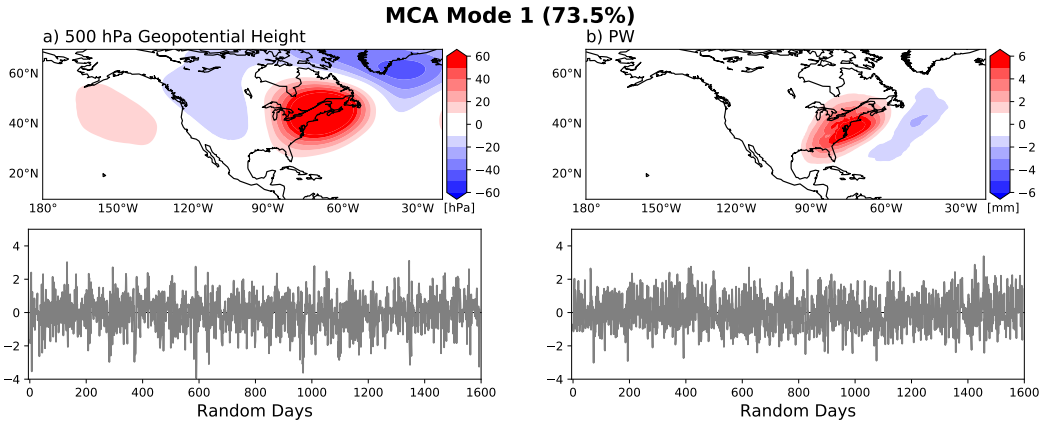


Figure A.8: Spatial patterns of geopotential height (left, a) and precipitable water (right, b) of the first mode of the MCA of 114 random non-events, with their respective time series of expansion coefficients under the spatial maps. Events are labeled based on if the event occurred within the NE wet or dry season.

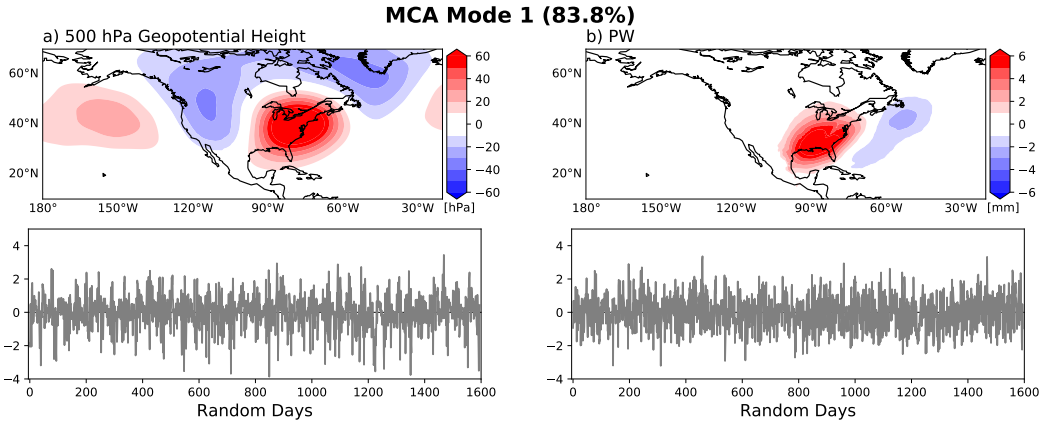


Figure A.9: As in Fig. A.8 but for the NE.

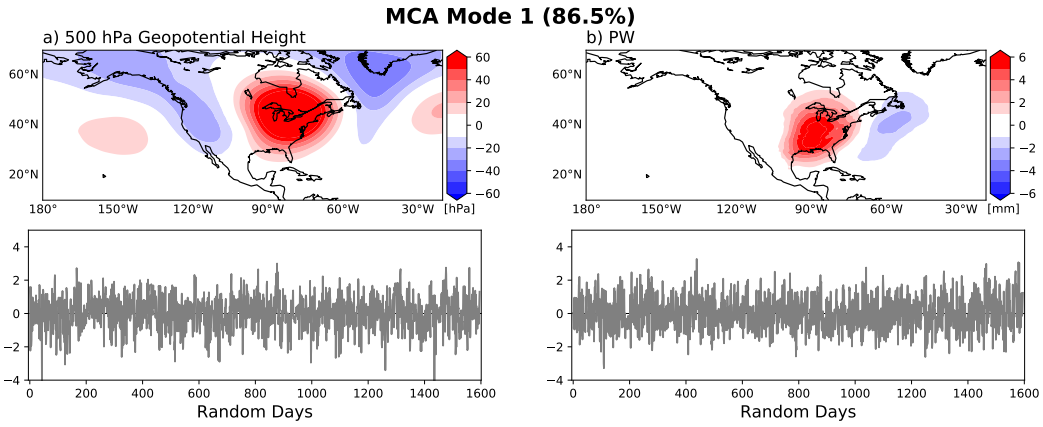


Figure A.10: As in Fig. A.8 but for the GL.

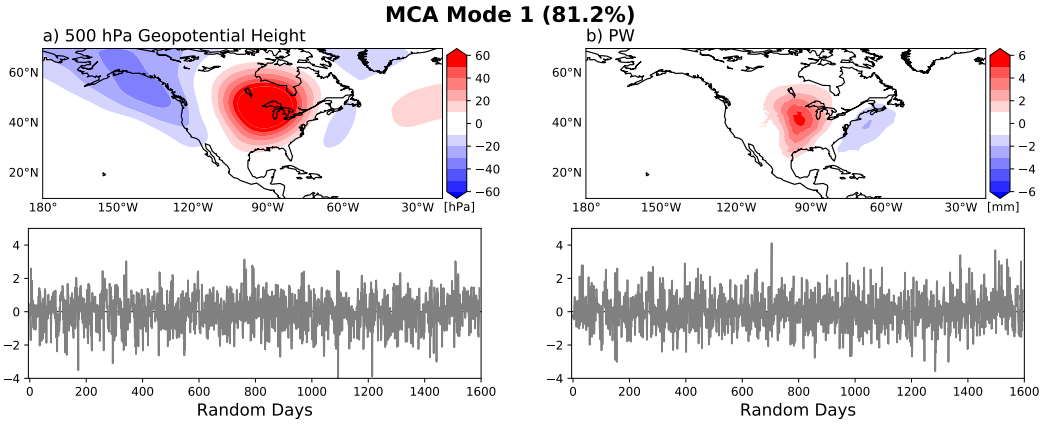


Figure A.11: As in Fig. A.8 but for the NP.

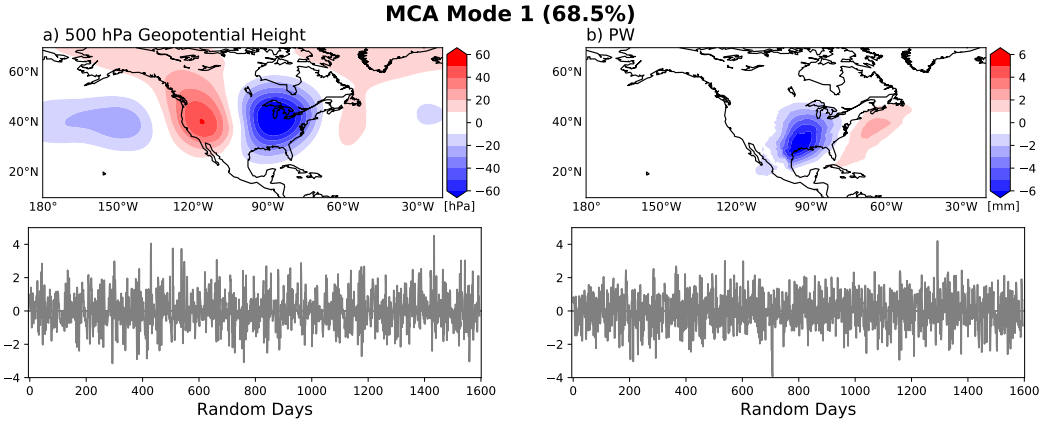


Figure A.12: As in Fig. A.8 but for the SP.

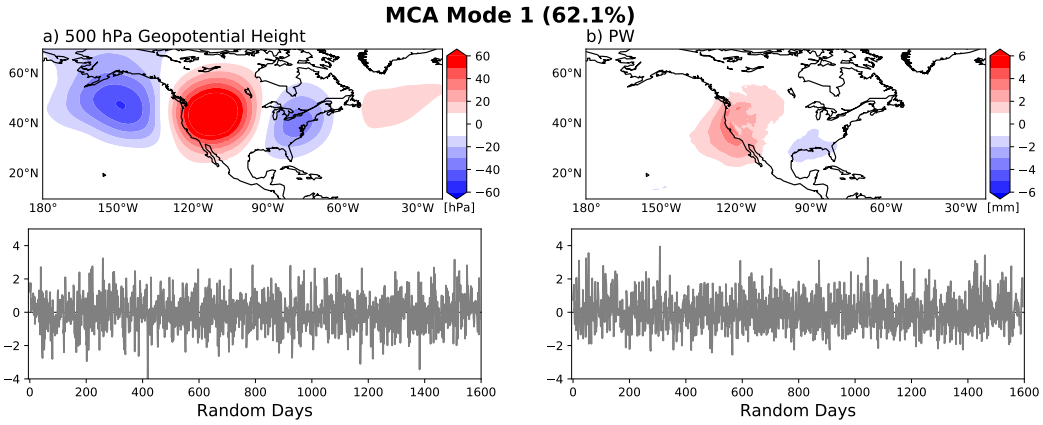


Figure A.13: As in Fig. A.8 but for the MW.

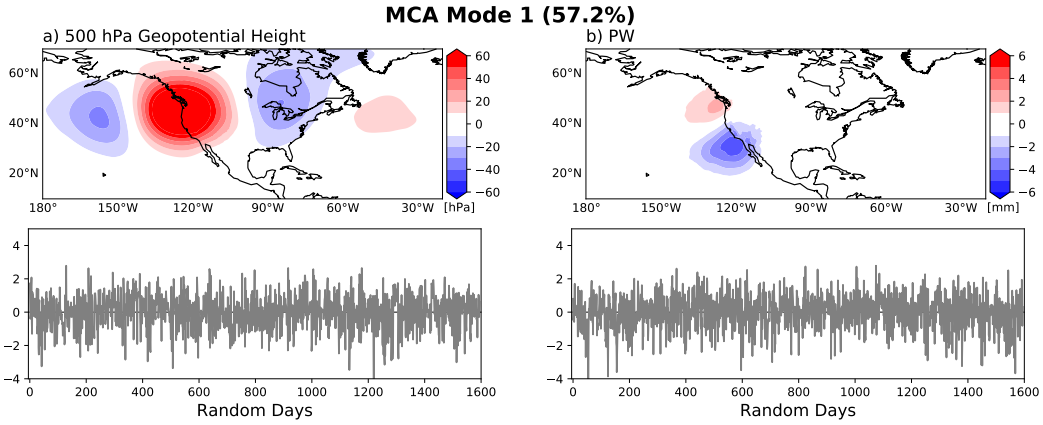


Figure A.14: As in Fig. A.8 but for the WC.